

## Structure-Based Design of Potent, Amidine-Derived Inhibitors of Factor Xa: Evaluation of Selectivity, Anticoagulant Activity, and Antithrombotic Activity

Michael R. Wiley,\* Leonard C. Weir, Steven Briggs, Nancy A. Bryan, John Buben, Charles Campbell, Nickolay Y. Chirgadze, Richard C. Conrad, Trelia J. Craft, James V. Ficorilli, Jeffry B. Franciskovich, Larry L. Froelich, Donetta S. Gifford-Moore, Theodore Goodson, Jr., David K. Herron, Valentine J. Klimkowski, Kenneth D. Kurz, Jeffery A. Kyle, John J. Masters, Andrew M. Ratz, Guy Milot, Robert T. Shuman, Tommy Smith, Gerald F. Smith, Ann Louise Tebbe, Jennifer M. Tinsley, Richard D. Towner, Alexander Wilson, and Ying K. Yee\*

Lilly Research Laboratories, Eli Lilly and Company, Indianapolis, Indiana 46285

Received June 24, 1999

To enhance the potency of 1,2-dibenzamidobenzene-derived inhibitors of factor Xa (fXa), an amidine substituent was incorporated on one of the benzoyl side chains to interact with Asp189 in the S1 specificity pocket. Lead molecule **1** was docked into the active site of fXa to facilitate inhibitor design. Subsequently, iterative SAR studies and molecular modeling led to a 1000-fold increase in fXa affinity and a refined model of the new inhibitors in the fXa active site. Strong support for the computational model was achieved through the acquisition of an X-ray crystal structure using thrombin as a surrogate protein. The amidines in this series show high levels of selectivity for the inhibition of fXa relative to other trypsin-like serine proteases. Furthermore, the fXa affinity of compounds in this series ( $K_{\text{ass}} = 50\text{--}500 \times 10^6 \text{ L/mol}$ ) translates effectively into both anticoagulant activity in vitro and antithrombotic activity in vivo.

### Introduction

The search for novel anticoagulant agents has emerged as one of the most active areas of current investigation in drug discovery.<sup>1</sup> This is due to the large number of patients afflicted each year with thrombotic diseases,<sup>2</sup> coupled with the therapeutic limitations of warfarin.<sup>3</sup> Several of warfarin's properties, such as an indirect mechanism of action, a susceptibility to drug–drug and drug–food interactions, and the need for frequent monitoring, contribute to the dissatisfaction with this agent. Much of the recent effort to find improved anticoagulants has been focused on the identification of compounds which, unlike warfarin, derive anticoagulant activity through direct and selective inhibition of coagulation enzymes. Of these enzymes, thrombin has been the most popular target, due to its central role in the control of clot formation.<sup>4</sup> However, recently more attention has been focused on the development of inhibitors of the enzymes which control thrombin generation.

Thrombin is produced via the coagulation cascade, a series of enzyme activation steps involving the serine proteases factor VIIa, factor IXa, and factor Xa.<sup>5</sup> In theory, all of these proteases are attractive targets for drug development, and in each case, antithrombotic efficacy has been demonstrated in animal models with selective, protein-based inhibitors.<sup>6–8</sup> To focus on one of these targets, we used a primary screening assay which generated hits for all of the enzymes in the extrinsic pathway simultaneously<sup>9</sup> and then used secondary assays to assign which enzyme was responsible for activity. The prioritization of biological targets was then determined on the basis of the properties of the

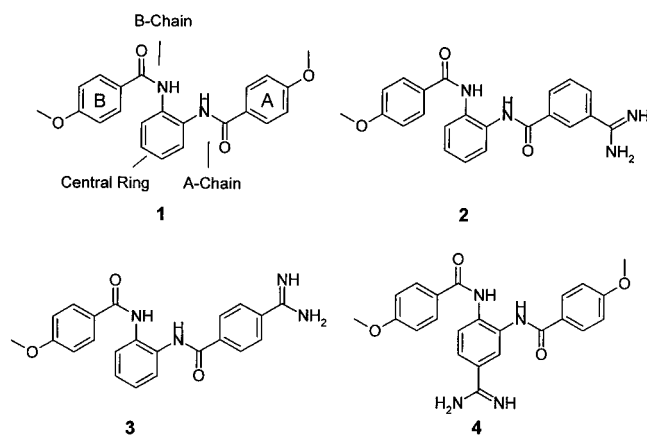
resulting chemical leads. This strategy led to the selection of factor Xa (fXa) as a target, due to the identification of the 1,2-dibenzamidobenzene derivative **1** (see Figure 1), a competitive inhibitor of fXa with an association constant of  $0.84 \times 10^6 \text{ L/mol}$  ( $K_i = 1.0 \mu\text{M}$ ).<sup>10</sup> The simple structure of **1** and its susceptibility to rapid SAR investigation made it an attractive candidate for further study.

### Inhibitor Design

One strategy which has been used for the development of potent thrombin inhibitors involves the use of aromatic amidines.<sup>11</sup> This approach relies on the strong interaction between a positively charged amidinium ion on the enzyme inhibitor and the side chain of Asp189, a poorly solvated carboxylate anion which sits in the S1 specificity pocket of the trypsin-like serine protease. Assuming compound **1** binds to the active site of fXa, we wanted to explore the incorporation of amidine substituents into the inhibitor in order to enhance interactions with the S1 site.

Other reports have also recently appeared describing the use of aromatic amidines in the development of small molecule inhibitors of fXa.<sup>12</sup> In many of these studies, the placement of an aromatic amidine in the S1 pocket was assumed due to the high degree of structural homology in the S1 sites of thrombin and fXa, and the resulting computational models provided the basis for further structural modifications. However since our lead compound (**1**) did not possess a positively charged group, its binding orientation in the active site of fXa was not immediately apparent. To develop hypotheses regarding which regions of the inhibitor might derive benefit from the introduction of an amidine

\* Corresponding authors. E-mail: wileymr@lilly.com and yee.ying.k@lilly.com.



**Figure 1.** Structures of lead fXa inhibitor **1** and prototypical amidines **2–4**.

substituent, computational models of **1** docked into the fXa active site were constructed.

Using the X-ray structure of human fXa-des(1–45) described by Padmanabhan et al.<sup>13</sup> as a starting point, the computational exploration of the fXa active site for potential binding modes of **1** was performed as described in the Experimental Section. Our goal in this study was to quickly generate a collection of plausible binding models which could be subjected to experimental testing through the design, synthesis, and biological evaluation of resulting target molecules. Therefore, the first stage of our docking studies utilized only a small number of reasonable conformations of **1**, and results were scored solely on the basis of complementary shape criteria. Three possible binding modes were suggested by this analysis, and a graphical representation of each is illustrated in Figure 2.

Visual inspection of the three models revealed that in each case, a different portion of inhibitor **1** was in close proximity to the carboxyl group of Asp189. Both model I and model II indicate that one of the *p*-methoxybenzoyl side chains of **1** occupies the S1 site on fXa. In model I, the *meta*-position of the S1 binding element points directly at Asp189. However in model II, the *para*-position of the side chain is directed toward the carboxylate. Finally, in model III the central ring of the inhibitor occupies the S1 site with the 4-position being nearest Asp189. To provide experimental data to support one or more of these computational models, compounds **2–4** (Figure 1) were targeted for synthesis and biological evaluation. In each case the amidine is incorporated at the position of inhibitor **1** which is closest to Asp189 in one of the three models.

Amidines analogues which provided an increase in enzyme affinity were then subjected to further computational refinement as described in the Experimental Section. These studies provided the basis for additional structure-based SAR studies to confirm how the remainder of the ligand may be positioned in fXa and to seek further enhancement of enzyme affinity through improved interactions with other regions of the protein.<sup>10,14</sup>

## Chemistry

The benzamidines described in this report were all prepared from benzonitrile intermediates. Scheme 1 illustrates the synthesis of those benzonitriles which

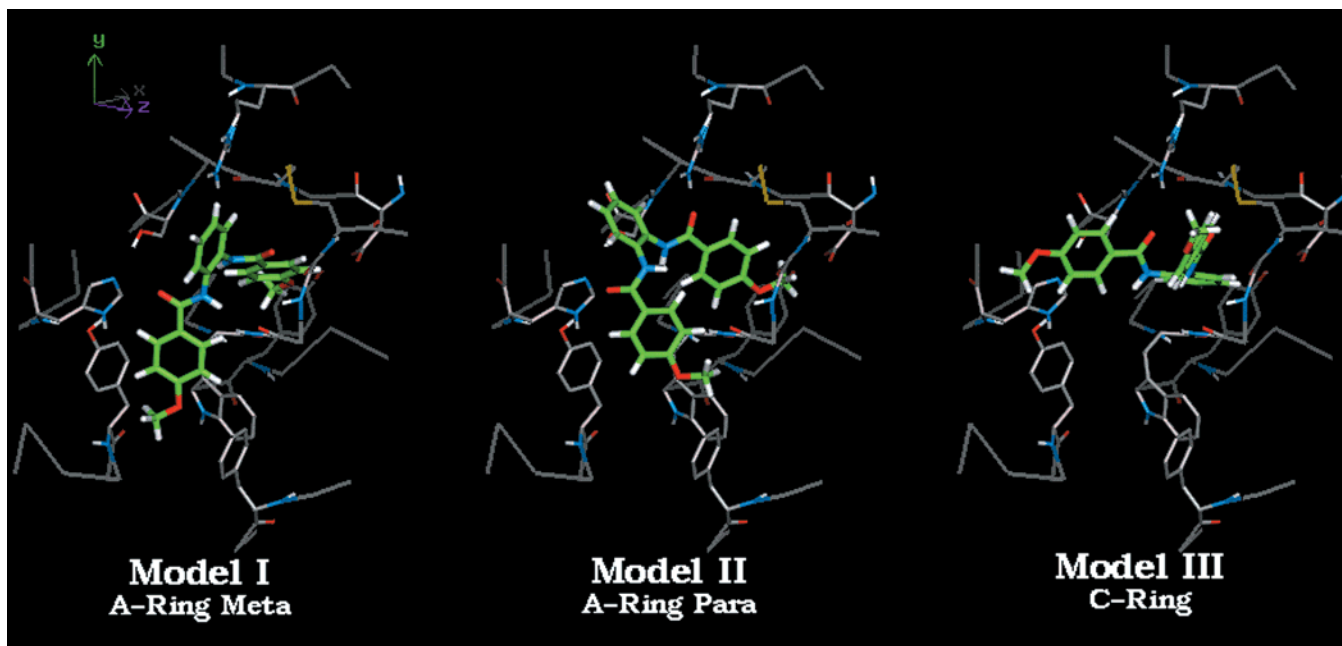
were derivatives of 1,2-dibenzamidobenzene (**19–28**), starting from either an *o*-nitroaniline (**5**, **6**) or a substituted 1,2-benzenediamine (**7**, **8**). In the *o*-nitroaniline approach, the first side chain was introduced through acylation of either **5** or **6** with a substituted benzoyl chloride to give compounds **9–12**. The nitro group was then reduced by catalytic hydrogenation to give anilines **13–16**. A second acylation with another substituted benzoyl chloride provided the diacylated intermediates **19–25**. Alternatively, methyl 1,2-benzenediamine-4-carboxylate (**7**) was selectively acylated on the amine *meta* to the ester, due to deactivation of the *p*-amine by the strong electron-withdrawing group. The resulting monoacylated diamines **17** and **18** were then treated with a second equivalent of acid chloride to give the diacylated derivatives **26** and **27**, respectively. Compound **28**, which bears the nitrile substituent on the central ring, was prepared simply by treatment of 3,4-diaminobenzonitrile (**8**) with 2 equiv of *p*-anisoyl chloride.

Scheme 2 illustrates the synthetic modifications which were performed on the central ring substituents of intermediates **25–27**. The TBS ether **25** was deprotected by treatment with TBAF, and the resulting phenol (**29**) was alkylated with either benzyl 2-bromoacetate to give compound **30** or ethyl 2-bromoacetate to give compound **31**. Methyl esters **26** and **27** were subjected to a two-step transesterification sequence, to give the benzyl esters **32** and **33**, respectively.

The fully assembled benzonitrile intermediates **19–24** and **29–33** were then elaborated to the amidine target molecules by one of two methods, as illustrated in Scheme 3. Compounds **19** and **20** were converted to amidines **2** and **3**, respectively, through the modified thio-Pinner sequence which has been recently described.<sup>15</sup> Alternatively, benzonitrile **28** was converted to amidoxime **34** by treatment with hydroxylamine and Hunig's base. The N–O bond of the amidoxime was then cleaved by catalytic hydrogenation to provide amidine **4**.<sup>16</sup> The remaining benzonitrile intermediates were all converted to amidines **44–52** via the amidoxime–hydrogenolysis route.

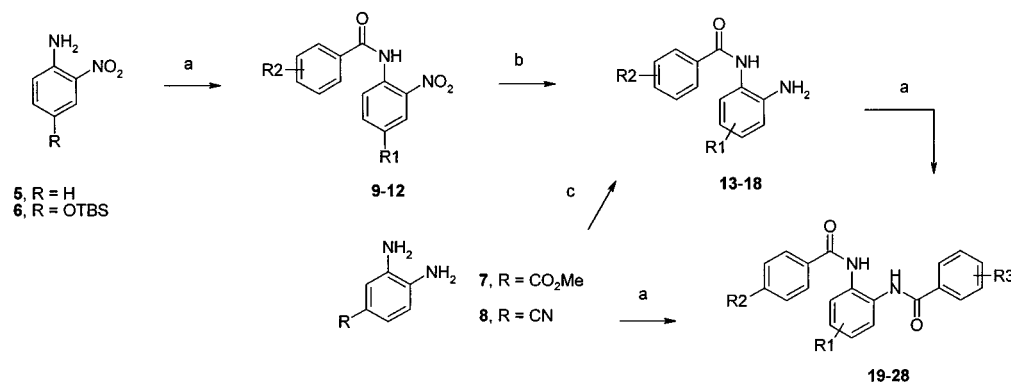
The methods used for the preparation of benzamidines derived from anthranilic acid-based intermediates (**57** and **62**) are illustrated in Scheme 4. The synthesis of compound **57** begins with the coupling of *p*-anisidine with isatoic anhydride (**53**) to give the anthranilamide derivative **54**. Treatment of **54** with *m*-cyanobenzoyl chloride provided the fully assembled benzonitrile intermediate **55**, which was modified as described above via the amidoxime **56** to produce amidine **57**. The synthesis of compound **62** was initiated by treatment of *m*-cyanoaniline with *o*-nitrobenzoyl chloride to give the *o*-nitrobenzamide derivative **58**. Reduction of the nitro group provided the anthranilamide **59**, which was acylated with 4-*tert*-butylbenzoyl chloride to give benzonitrile **60** and then converted to the amidine **62** by treatment with hydroxylamine followed by hydrogenation.

Scheme 5 illustrates the synthesis of amidine **68**, which incorporated a heterocyclic central ring. The synthesis of **68** began with acylation of methyl 3-aminothiophene-2-carboxylate (**63**) to give the benzamide derivative **64**. Compound **64** was hydrolyzed to give



**Figure 2.** Initial, unrefined binding modes for **1** (green) in the active site of fXa. The orientation of each model places Asp189 of the S1 pocket near the upper right-hand corner and the S4 aryl binding region in the lower center. The amidine isomer suggested by each model is noted.

### Scheme 1<sup>a</sup>



Compound	R1	R2	Compound	R1	R2	R3
9	H	4-OMe	19	H	OMe	3-CN
10	H	4-t-Bu	20	H	OMe	4-CN
11	H	3-CN	21	H	t-Bu	3-CN
12	OTBS	3-CN	22	H	t-Bu	4-CN
13	H	4-OMe	23	H	OEt	3-CN
14	H	4-t-Bu	24	H	i-Pr	3-CN
15	H	3-CN	25	4-OTBS	i-Pr	3-CN
16	5-OTBS	3-CN	26	4-COOMe	t-Bu	3-CN
17	4-COOMe	4-t-Bu	27	5-COOMe	t-Bu	3-CN
18	4-COOMe	3-CN	28	4-CN	OMe	4-OMe

<sup>a</sup> (a) R-BzCl, pyridine, CH<sub>2</sub>Cl<sub>2</sub>; (b) H<sub>2</sub>, 10% Pd/C, ethyl acetate; (c) R-BzCl, pyridine, acetonitrile, 0 °C.

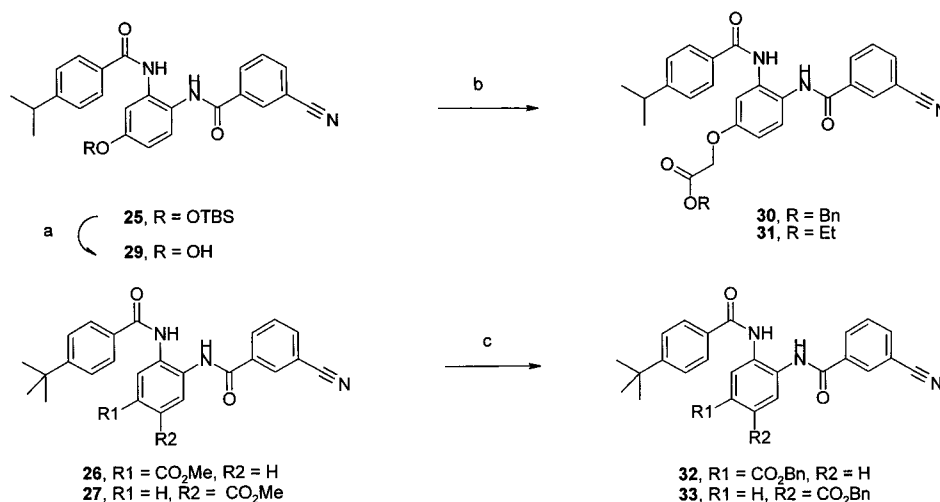
carboxylic acid **65** and then treated with oxalyl chloride to give the cyclic oxazinone derivative **66**. A ring-opening reaction was then performed by treatment of **66** with the potassium salt of *m*-cyanoaniline to give the benzonitrile derivative **67**, which was elaborated to amidine **68** through the modified thio-Pinner sequence.

Finally, Scheme 6 illustrates the synthesis of two compounds (**71** and **72**) in which the amidine is incorporated into a nonaromatic A-ring. The synthesis begins by coupling the bis(Cbz)-*S*-methylisothiourea (**69**) with nipecotic acid to give the *N*-protected amidinonipecotic acid derivative **70**. Acid **70** was then coupled with

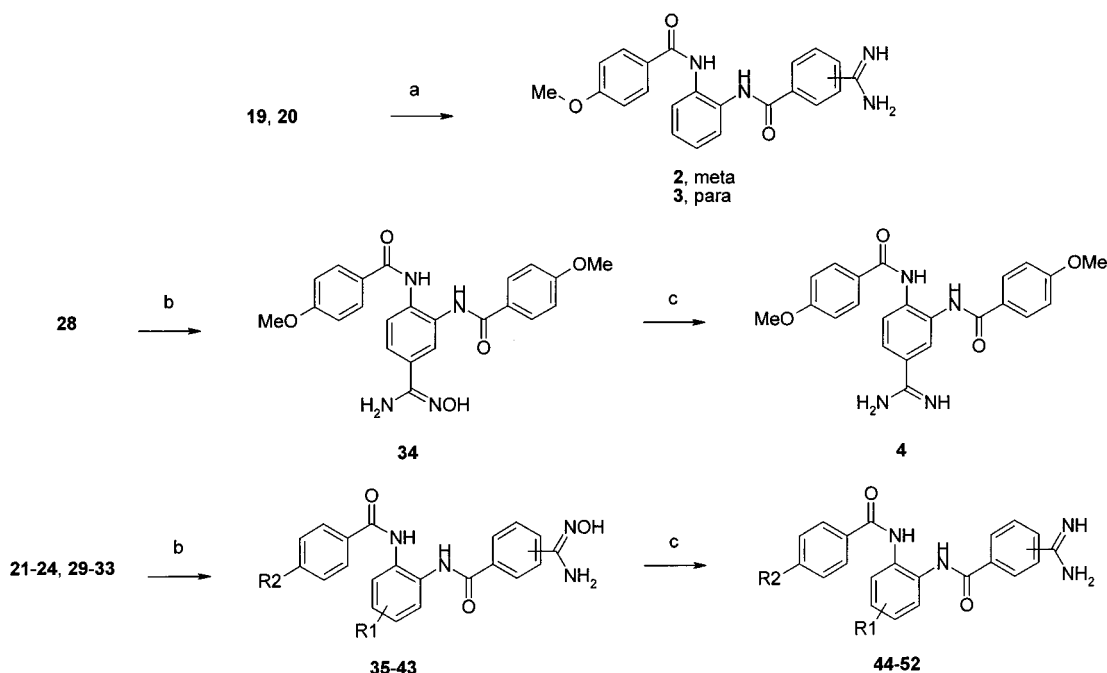
monoacylated diaminobenzene **13** or **14**, followed by deprotection to give amidine **71** and **72**, respectively.

### Results and Discussion

**fXa Affinity and Molecular Modeling.** The data in Table 1 illustrate that a 17-fold increase in affinity results from the replacement of the *p*-methoxy substituent on one of the side chains of **1** with an amidine at the *meta*-position (**2**,  $K_{\text{ass}} = 14 \times 10^6$  L/mol,  $K_i = 30 \pm 1.7$  nM). A 7-fold increase in activity accompanies the incorporation of an amidine at the *para*-position of the side chain (**3**). The placement of an amidine on the

Scheme 2<sup>a</sup>

<sup>a</sup> (a) TBAF, THF; (b) BrCH<sub>2</sub>CO<sub>2</sub>R, K<sub>2</sub>CO<sub>3</sub>, acetone; (c) (i) LiOH, H<sub>2</sub>O/MeOH/THF (1/1/3), (ii) BnBr, K<sub>2</sub>CO<sub>3</sub>, DMF.

Scheme 3<sup>a</sup>

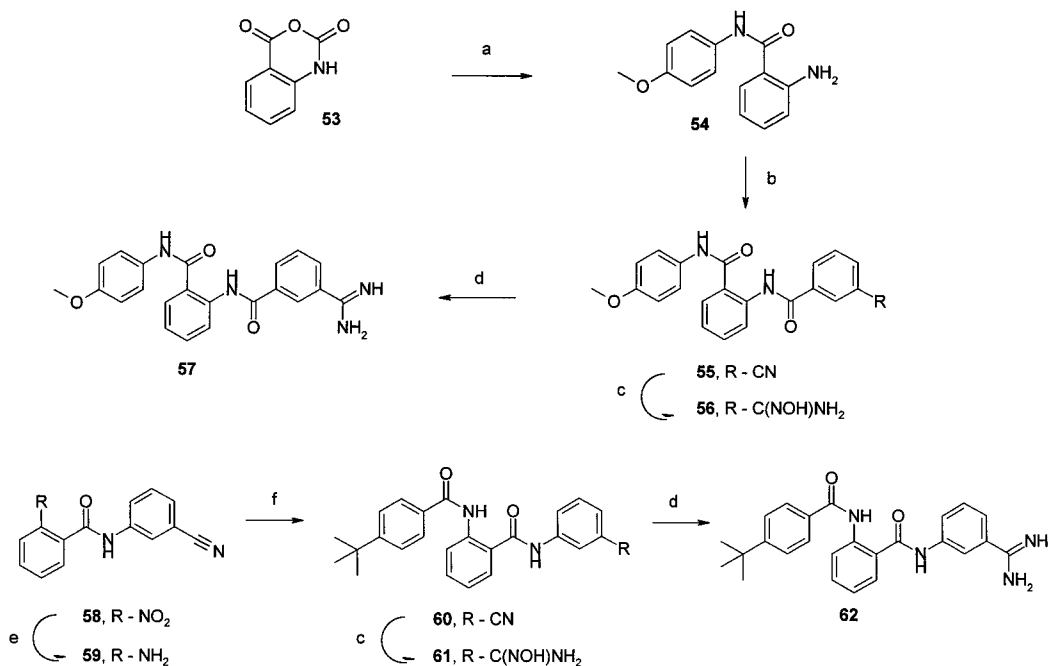
Compound	R1	R2	Amidoxime Isomer	Compound	R1	R2	Amidine Isomer
<b>35</b>	H	t-Bu	meta	<b>44</b>	H	t-Bu	meta
<b>36</b>	H	t-Bu	para	<b>45</b>	H	t-Bu	para
<b>37</b>	H	OEt	meta	<b>46</b>	H	OEt	meta
<b>38</b>	H	i-Pr	meta	<b>47</b>	H	i-Pr	meta
<b>39</b>	4-OH	i-Pr	meta	<b>48</b>	4-OH	i-Pr	meta
<b>40</b>	4-OCH <sub>2</sub> COOBn	i-Pr	meta	<b>49</b>	4-OCH <sub>2</sub> COOH	i-Pr	meta
<b>41</b>	4-OCH <sub>2</sub> COOEt	i-Pr	meta	<b>50</b>	4-OCH <sub>2</sub> COOEt	i-Pr	meta
<b>42</b>	4-COOBn	t-Bu	meta	<b>51</b>	4-COOH	t-Bu	meta
<b>43</b>	5-COOBn	t-Bu	meta	<b>52</b>	5-COOH	t-Bu	meta

<sup>a</sup> (a) (i) H<sub>2</sub>S, pyridine, (ii) MeI, acetone, Δ, (iii) NH<sub>4</sub>OAc, MeOH, Δ, (iv) Boc<sub>2</sub>O, (v) TFA; (b) NH<sub>2</sub>OH·HCl, *i*-Pr<sub>2</sub>NEt, ethanol, Δ; (c) H<sub>2</sub>, 10% Pd/C, aq HCl, ethanol.

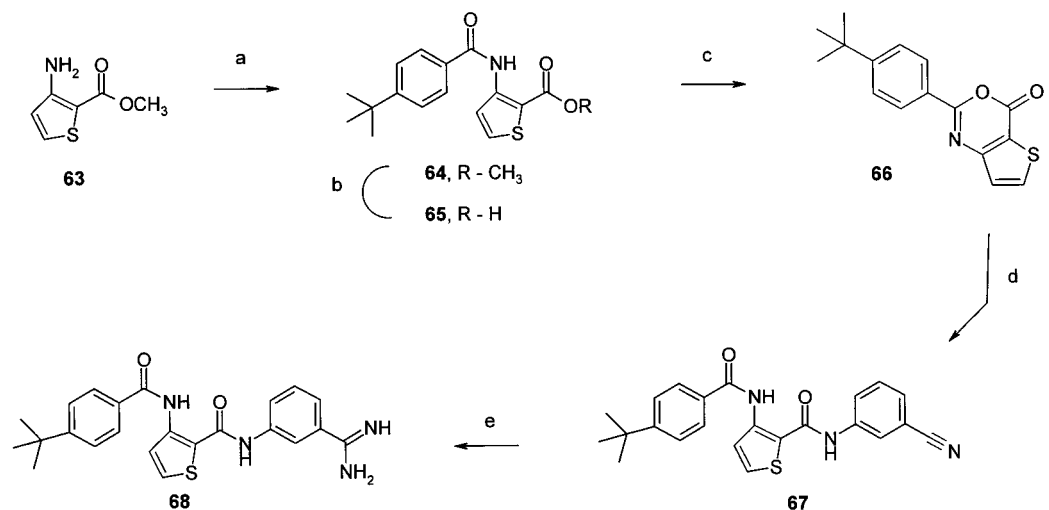
central ring (**4**) is detrimental. These data provide some support for the hypotheses illustrated in models I and II that the amidinobenzoyl side chains in compounds **2** and **3** serve as S1 binding elements.

Figure 3 illustrates the overlaid energy-minimized structures for the fXa active site complexes of compounds **2** (green) and **3** (purple). Both compounds are

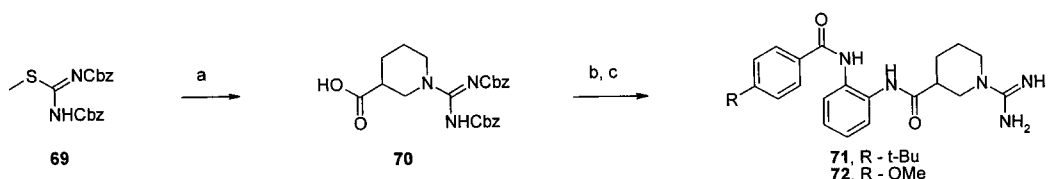
positioned such that the amidine-bearing side chain occupies the S1 pocket and the *p*-methoxybenzoyl side chain binds into the S4 pocket. Also, the central ring in each complex is predominately exposed, lying near Gly218, at the entrance to the S1 region. However, there are subtle structural differences in the proposed binding modes of **2** and **3** which may help to rationalize why

Scheme 4<sup>a</sup>

<sup>a</sup> (a) 4-Anisidine, toluene,  $\Delta$ ; (b) 3-CN-BzCl, pyridine, CH<sub>2</sub>Cl<sub>2</sub>; (c) NH<sub>2</sub>OH·HCl, *i*-Pr<sub>2</sub>NEt, ethanol,  $\Delta$ ; (d) H<sub>2</sub>, 10% Pd/C, aq HCl, ethanol; (e) H<sub>2</sub>, 10% Pd/C, ethyl acetate; (f) 4-*t*-Bu-BzCl, pyridine, CH<sub>2</sub>Cl<sub>2</sub>.

Scheme 5<sup>a</sup>

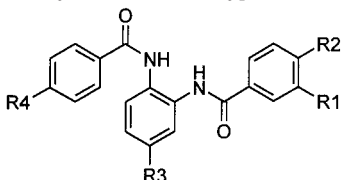
<sup>a</sup> (a) 4-*t*-Bu-BzCl, pyridine, CH<sub>2</sub>Cl<sub>2</sub>; (b) NaOH, aq dioxane; (c) oxalyl chloride, pyridine, CH<sub>2</sub>Cl<sub>2</sub>; (d) 3-cyanoaniline, KHMDS, THF; (e) (i) H<sub>2</sub>S, pyridine, (ii) MeI, acetone,  $\Delta$ , (iii) NH<sub>4</sub>OAc, MeOH,  $\Delta$ , (iv) Boc<sub>2</sub>O, (v) TFA.

Scheme 6<sup>a</sup>

<sup>a</sup> (a) Nipectic acid, NaOH, aq dioxane; (b) **13** or **14**, DCC, HOAT, CH<sub>2</sub>Cl<sub>2</sub>; (c) H<sub>2</sub>, 10% Pd/C, aq HCl, ethanol.

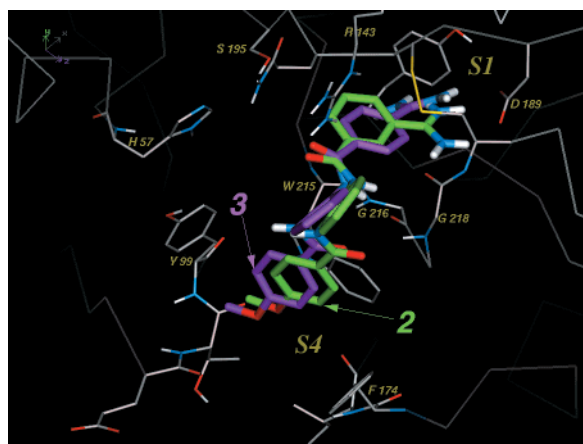
the *m*-amidinobenzoyl substituent is a more effective S1 binding element in this series. In the complex of **2**, the amide group which connects the benzamide to the central ring (A-chain, see Figure 1) is oriented such that the NH can donate a hydrogen bond to the backbone carbonyl oxygen of either Gly216 or Gly218. The equivalent A-chain amide in **3** is able to form a hydrogen bond

only to the carbonyl oxygen of Gly216. Also, the carbonyl oxygen of the B-chain amide in **2** may accept a hydrogen bond from the backbone NH of Gly218; however this is not observed for **3**. The *m*-amidine in **2** is in position to form an effective salt bridge with the carboxylate of Asp189, as well as hydrogen bond to the backbone carbonyl of Gly218. The hydrogen bond formed by the

**Table 1.** fXa Affinity Data for Prototypical Amidines


Compound	R1	R2	R3	R4	fXa $K_{\text{ass}}^a$
1	-H	-OMe	-H	-OMe	0.84
2		-H	-H	-OMe	14.
3	-H		-H	-OMe	5.7
4	-H	-OMe		-OMe	0.27

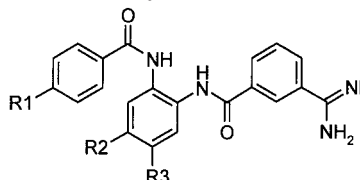
<sup>a</sup>  $K_{\text{ass}}$  is the apparent association constant reported in units of  $10^6$  L/mol and is approximately equal to  $1/K_i$  (see Experimental Section). All values are the average of at least 3 separate experiments with a standard deviation of less than 15%.



**Figure 3.** Energy-minimized binding models of the amidine-substituted analogues **2** (*meta*, green) and **3** (*para*, purple) complexed with the active site of fXa. The active site residues shown are from the energy-minimized complex of **2**. Only the ligand is shown for the complex of **3** (equivalently processed). In this orientation, Asp189 appears in the upper right-hand corner, Ser195 near the top central, and Glu97 in the lower left-hand corner. All aliphatic hydrogens and waters have been removed for clarity.

*p*-amidine in **3** appears to have a less than optimal geometric orientation<sup>17</sup> relative to Asp189, and it rotates 40° out of the plane of the aromatic ring compared to 12° in the model of **2**.

In the next iteration, we sought to combine the benzamidine S1 binding elements with functional groups designed to improve interactions between the inhibitor and neighboring binding sites on fXa. Results reported in our previous paper<sup>10</sup> revealed that the incorporation of a *tert*-butyl group at the *para*-position of one of the side chains of compound **1** significantly increased fXa affinity, presumably through an improved interaction with the S4 site on the enzyme. The 18-fold increase in fXa inhibitory activity found with compound **44** (relative to **2**, Table 2) illustrates the benefit which can be provided by an appropriately placed *tert*-butylphenyl substituent in combination with a *m*-benzamidine. However, the opposite effect was observed with the

**Table 2.** Structure–Activity Data for *m*-Amidines


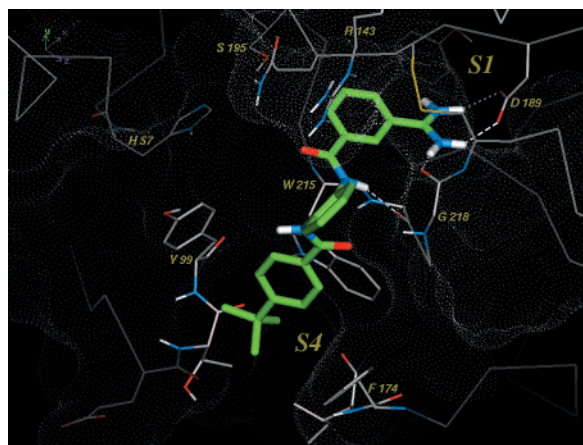
Compound	R1	R2	R3	fXa $K_{\text{ass}}^a$
2	-OMe	-H	-H	14.
44	- <i>t</i> -Bu	-H	-H	250.
46	-OEt	-H	-H	29.
47	- <i>i</i> -Pr	-H	-H	180.
48	- <i>i</i> -Pr	-OH	-H	230.
49	- <i>i</i> -Pr	-OCH <sub>2</sub> CO <sub>2</sub> H	-H	340.
50	- <i>i</i> -Pr	-OCH <sub>2</sub> CO <sub>2</sub> Et	-H	160.
51	- <i>t</i> -Bu	-H	-CO <sub>2</sub> H	54.
52	- <i>t</i> -Bu	-CO <sub>2</sub> H	-H	470.

<sup>a</sup>  $K_{\text{ass}}$  is the apparent association constant reported in units of  $10^6$  L/mol and is approximately equal to  $1/K_i$  (see Experimental Section). All values are the average of at least 3 separate experiments with a standard deviation of less than 15%.

*p*-amidine **45** ( $K_{\text{ass}} = 0.02 \times 10^6$  L/mol), which suffered a 300-fold loss in fXa affinity relative to **3**. In this particular case, the difference may be rationalized by the modeling observation that the *p*-amidine, besides binding in a conformationally strained orientation within the S1 pocket, also may restrict B-chain placement within the S4 region. Figure 3 shows that the *p*-methoxybenzoyl group in **3** is not as centrally located within the S4 binding region as is the equivalent group in **2**. Therefore, the bulkier *tert*-butyl group is poorly accommodated in the S4 binding site when combined with the less-optimal amidine orientation at the S1 site. The same substitution in the *m*-amidine (**44**) appears to favorably increase the hydrophobic surface area in contact between the ligand and the three aromatic side chains that frame the S4 region.

The energy-minimized structure for the fXa active site complex of **44** is shown in Figure 4. The hydrogen-bonding interactions for **44** with various active site residues are essentially equivalent to those previously described for **2**. Note that the *tert*-butyl group is centrally located within the highly hydrophobic S4 region.

The results of additional SAR studies, focused on the *m*-amidine series, are provided in Table 2. These results provide additional support for the computational model described above as an appropriate representation of the binding orientation of this series of compounds in the active site of fXa. The relative activity of compounds **2** (R1 = OMe), **46** (R1 = OEt), **47** (R1 = *i*-Pr), and **44** (R1 = *t*-Bu) shows that fXa affinity increases as the size of the *para*-substituent increases to fill the hydrophobic S4 site. The activity of the central ring-modified compounds in Table 2 demonstrates that some additional binding energy can also be derived from the appropriate placement of acidic residues on the central ring. While placement of the carboxy substituent in the 5-position



**Figure 4.** Energy-minimized binding model of compound **44** complexed with the active site of fXa. The orientation of the complex is the same as in Figure 3. The active site molecular surface is highlighted by small white dots, and hydrogen bonds between **44** and the protein are shown as dashed lines.

of the central ring (**51**) decreased activity relative to compound **44** by about a factor of 5, moving the carboxy group to the 4-position (compound **52**) gave about a 2-fold increase in activity, with an association constant of 470 million.

The importance of connecting the S1 and S4 binding elements with an appropriate structural element is illustrated by the data in Table 3. Compounds **57**, **62**, and **68** demonstrate that reversing the position of the amide connecting either side chain to the central ring results in a 10–50-fold loss in activity. This stands in contrast to the results observed for neutral S1 binding elements, where reversing the orientation of the A-chain amide was well-tolerated.<sup>14</sup> Finally, planarity of the A-ring also seems to be important as the amidinopiperidine derivatives **71** and **72** sustain a 10–20-fold loss in affinity relative to the corresponding benzamidines.

**X-ray Structure of the 44–Thrombin Complex.** Although the computational model represented in Figures 3 and 4 is consistent with the SAR results shown in Tables 1–3, we sought additional physical chemical evidence to support this proposed modeling hypothesis. To provide this evidence, and to strengthen the structural basis for further molecular modeling, experimental crystallographic data was pursued. Unfortunately, initial crystallization experiments with complexes of fXa and several of the more potent compounds from Tables 1 and 2 were unsuccessful. As an alternative strategy, we looked for an opportunity to cocrystallize one of the inhibitors with a homologous serine protease.

Published X-ray structures of thrombin<sup>18</sup> and trypsin<sup>19</sup> demonstrate that both of these enzymes have a very high degree of structural homology with fXa in the S1 binding region. Furthermore, thrombin and trypsin also have well-defined hydrophobic S4 sites, although in these proteins this region has less aromatic character than in fXa. Recently, a similar surrogate strategy for structure-based design was reported using trypsin complexes of fXa inhibitors.<sup>20</sup> We chose to pursue thrombin as the surrogate protease as a result of our previous experience with preparing crystals of thrombin in complex with small molecule inhibitors.<sup>21</sup> After evaluation of the serine protease selectivity profile for several analogues (see below), compound **44** was identi-

**Table 3.** Alternative Central Rings and Nonaromatic Amidines

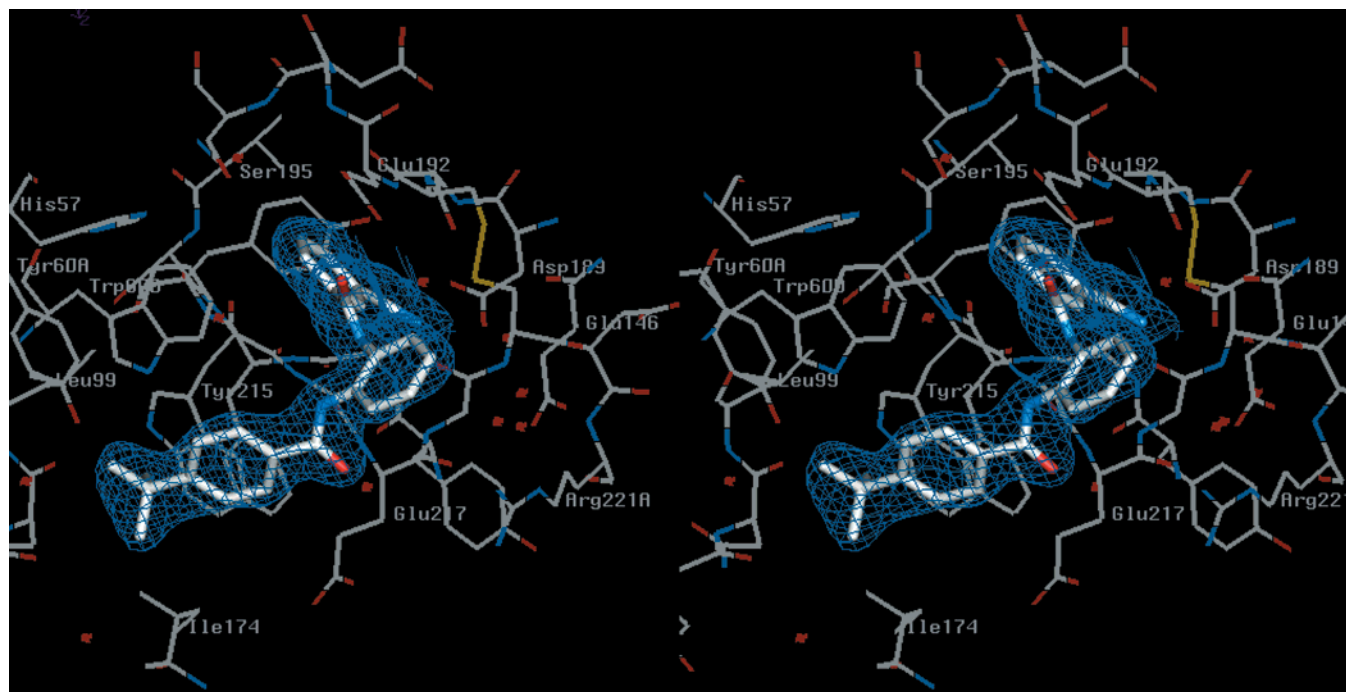
Compound	Structure	fXa $K_{\text{ass}}^a$
<b>57</b>		1.7
<b>62</b>		3.5
<b>68</b>		12.
<b>71</b>		12.0
<b>72</b>		1.0

<sup>a</sup>  $K_{\text{ass}}$  is the apparent association constant reported in units of  $10^6$  L/mol and is approximately equal to  $1/K_i$  (see Experimental Section). All values are the average of at least 3 separate experiments with a standard deviation of less than 15%.

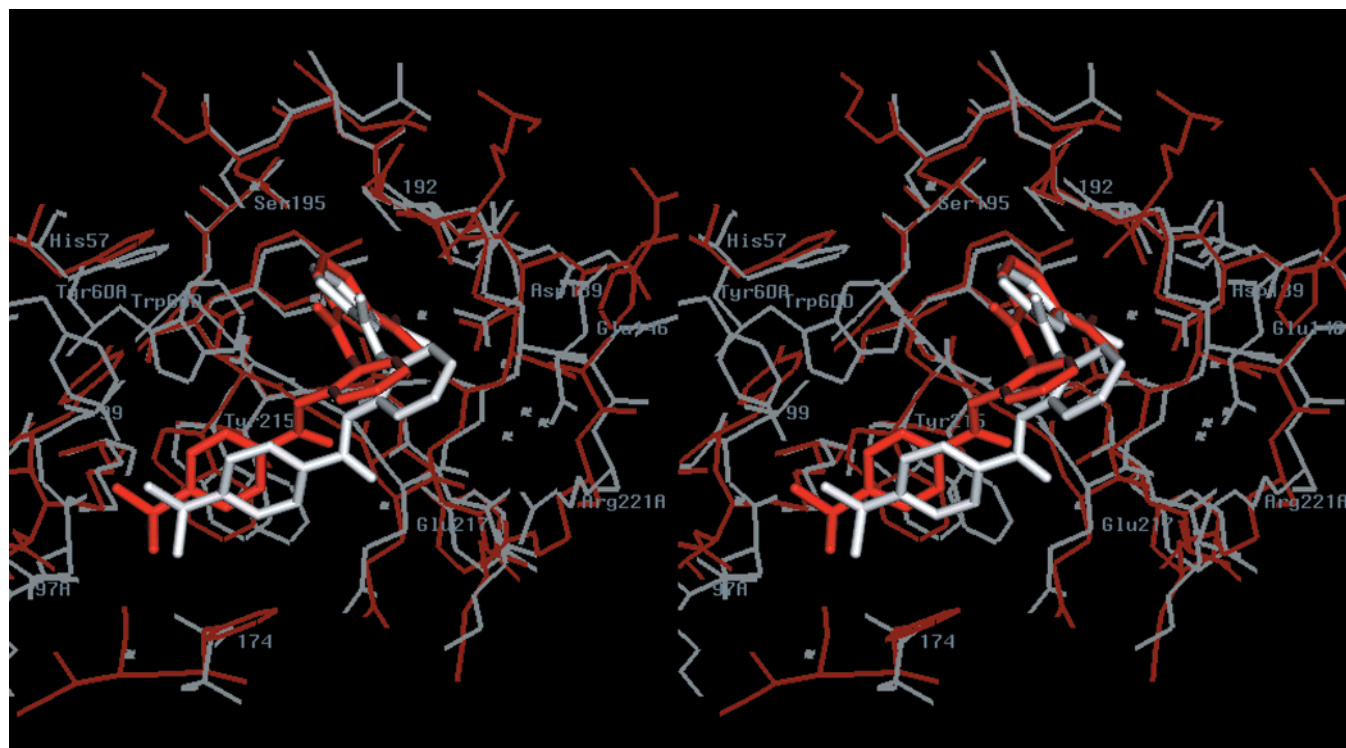
fied as the best candidate for cocrystallization based on its thrombin affinity ( $K_{\text{ass}}$  of  $3.0 \times 10^6$  L/mol). After preparing crystals using methods previously described,<sup>21</sup> the X-ray structure of compound **44** in complex with human  $\alpha$ -thrombin and the exo-site-bound peptide hirugen was determined at 2.1 Å resolution. Details on the data collection and crystallographic refinement are found in the Experimental Section.

As shown in Figure 5, the binding of the inhibitor in thrombin is characterized by two sites of interaction. The first places the benzamidine ring into the S1 specificity pocket so that the amidine forms a salt bridge with Asp189. It may also simultaneously form a hydrogen bond to the carbonyl of Gly219 (Gly218 in fXa). The A-chain amide linkage is in position to donate a hydrogen bond to the carbonyl of Gly216. The *tert*-butylphenyl group of the B-chain binds into the shallow hydrophobic S3/S4 binding region formed by Leu99, Trp215, and Ile174 (Tyr99, Trp215, and Phe174, respectively in fXa). One edge of the central ring of compound **44** resides in a hydrophobic region framed by Gly219, Cys220, and the side chain of Glu146, while the opposite edge is exposed to solvent. No significant interactions with the unique thrombin S2 binding site or the catalytic residues are observed.

Appearing in Figure 6 is an overlay of the experimental X-ray structure of the complex of **44** with thrombin (white) and the computationally modeled complex of **44** with fXa (red). This was achieved by aligning the sequences and then performing a least-squares fit to superimpose the  $\alpha$ -carbon of all identical residues. Although a strict comparison of the two systems is complicated by many factors, it is still interesting to note



**Figure 5.** Stereoview of compound **44** bound to the active site of human  $\alpha$ -thrombin. Blue mesh represents electron density that corresponds to the inhibitor. The  $\sigma_A$  electron density map was calculated for the 2.0–2.1 Å resolution range and countered at the  $1.0\sigma$  level.



**Figure 6.** Stereoview superposition of the active site complexes of **44** bound to both thrombin and fXa. The experimental X-ray structure of thrombin (2.1 Å resolution) is shown in white, and the computationally derived fXa structure is shown in red.

the similarities and differences. The overlay shows agreement in the overall binding modes. Furthermore, all of the previously described binding features (hydrogen bonds and hydrophobic interactions) are accounted for. The differences appear to reside predominately in the positions of the central ring and the B-chain. In the experimental thrombin complex, the central ring appears to reside closer to the residues that make up the entrance to the S1 pocket. Thus, the central ring

appears to be less exposed to solvent when compared to the corresponding modeled fXa structure. For the B-chain, in the thrombin complex the ligand does not sit as deeply in the S4 region as the corresponding B-chain in the fXa model. Also in the thrombin structure, the B-chain is at a more obtuse dihedral angle with respect to the central ring (C1–C2–N–C = 129°) than in fXa (68°). This conformational feature makes it unlikely that the B-chain carbonyl will form a hydrogen

**Table 4.** Serine Protease Selectivity Profile

compd	fXa	enzyme $K_{\text{ass}}^a$ /(selectivity ratio) <sup>b</sup>					
		thrombin	trypsin	plasmin	tPA	UK	aPC
2	14	0.27	0.60	0.020	0.020	0.001	0.015
		(56)	(25)	(750)	(750)	(15000)	(1000)
44	250	3.0	0.34	0.006	0.011	0.000	0.002
		(83)	(740)	(42000)	(23000)	(>250000)	(13000)
49	340	0.80	2.5	0.039	0.007	0.001	0.014
		(430)	(140)	(8700)	(49000)	(340000)	(24000)
52	470	0.65	12	0.073	0.004	0.001	0.013
		(720)	(390)	(6400)	(12000)	(470000)	(36000)

<sup>a</sup>  $K_{\text{ass}}$  is the apparent association constant reported in units of  $10^6$  L/mol and is approximately equal to  $1/K_i$  (see Experimental Section). All values are the average of at least 3 separate experiments with a standard deviation of less than 15%. <sup>b</sup> Selectivity ratio represents the fXa  $K_{\text{ass}}$ /enzyme  $K_{\text{ass}}$ .

**Table 5.** In Vitro Anticoagulant Activity

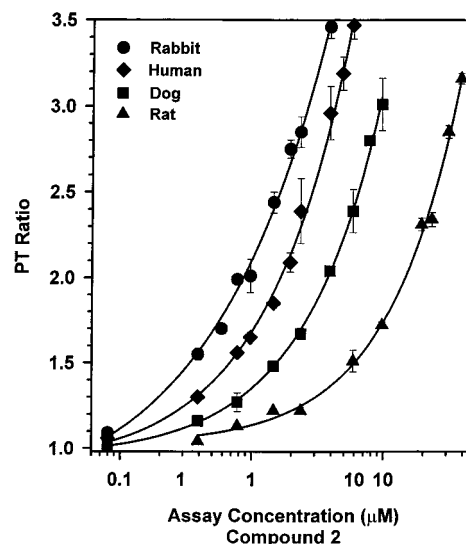
compd	$2 \times \text{APTT}$ ( $\mu\text{M}$ ) <sup>a</sup>	$2 \times \text{PT}$ ( $\mu\text{M}$ ) <sup>a</sup>
2	2.0	1.5
44	0.67	0.96
52	0.72	0.83
D-1-Piq-Pro-ArgH	1.2	2.9

<sup>a</sup> Activity is defined as the concentration of test compound required to double the time to clot formation in reconstituted human plasma, using either the activated partial thromboplastin time assay (APTT) or the prothrombin time assay (PT) as described in the Experimental Section.

bond to the NH of Gly219 in thrombin as opposed to in the equivalent residue in fXa (Gly218). So although there are subtle differences in the binding orientation of compound 44 in complex with thrombin relative to the proposed orientation of the inhibitor in fXa, the similarities in the two structures do provide additional support for the computational model.

**Serine Protease Selectivity Profile.** The trypsin-like serine protease selectivity profiles for several compounds from this series are listed in Table 4. Of greatest concern is the magnitude of selectivity for the inhibition of fXa relative to the fibrinolytic enzymes (plasmin, t-PA, and urokinase) and activated protein C, since concomitant inhibition of these enzymes could compromise the ability of anticoagulants to achieve useful antithrombotic activity in vivo.<sup>22</sup> Fortunately, very high selectivity (3–4 orders of magnitude) is observed for the inhibition of fXa relative to all of these enzymes. In general, the compounds also demonstrate 2–3 orders of magnitude selectivity for the inhibition of fXa relative to thrombin and trypsin as well. A comparison of the selectivity ratios of compound 2 with compounds 44, 49, and 52 reveals that optimizing the interaction of the *p*-alkyl substituent on the B-ring of the inhibitor with the S4 site on fXa significantly enhances selectivity for the inhibition of fXa relative to the fibrinolytic enzymes. Comparing the ratios for compound 44 versus 49 and 52 illustrates that the incorporation of an acidic functional group on the central ring can be used to enhance selectivity for fXa relative to thrombin. Daiichi reported similar results and proposed that selectivity for fXa over thrombin resulted from a repulsive interaction between acidic functional groups on the inhibitor and the side chain of Glu192 in the active site of thrombin.<sup>23</sup>

**Anticoagulant and Antithrombotic Activity.** The coagulation profiles for several representative amidines are listed in Table 5. The data demonstrate that the fXa



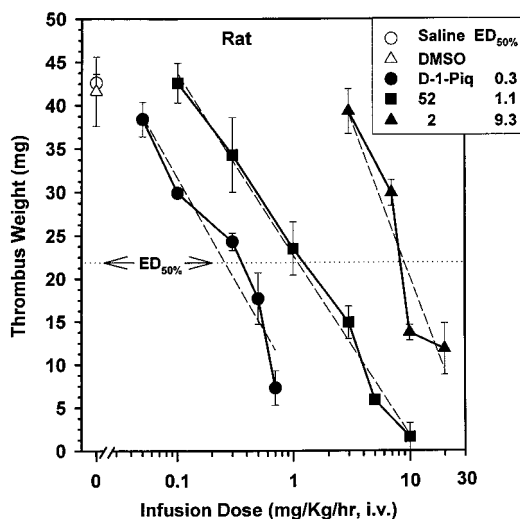
**Figure 7.** Concentration–response relationship of the prothrombin time (PT) ratio for compound 2 in plasma from various species. The  $2 \times$  assay concentrations ( $\mu\text{M}$ ) were as follows: rabbit,  $0.89 \pm 0.04$ ; human,  $1.7 \pm 0.09$ ; dog,  $3.8 \pm 0.23$ ; and rat,  $14.7 \pm 0.49$  ( $n = 3$  determinations/species).

affinity of the inhibitors translates very effectively into anticoagulant activity. With an association constant of  $14 \times 10^6$  L/mol, compound 2 doubles the PT at  $1.5 \mu\text{M}$  and the APTT at  $2.0 \mu\text{M}$ . As fXa affinity increases, anticoagulant activity is achieved at lower plasma concentrations of inhibitor. The more potent amidines such as compounds 44 and 52 double the PT and APTT at concentrations between  $0.6$  and  $1.0 \mu\text{M}$ .

The significance of this level of anticoagulant activity is illustrated by the comparison of compounds 2, 44, and 52 with D-1-Piq-Pro-ArgH<sup>24</sup> (Table 5), a tripeptide thrombin inhibitor which was evaluated in clinical trials. With a thrombin association constant of  $530 \times 10^6$  L/mol, D-1-Piq-Pro-ArgH doubles the PT and APTT in human plasma at concentrations of  $2.9$  and  $1.2 \mu\text{M}$ , respectively. Even the least potent amidine in this series (compound 2) achieves similar anticoagulant activity in human plasma.

Although the amidines achieve potent anticoagulant activity in human plasma, the use of thrombosis models to predict the relative potency of these inhibitors with other anticoagulant agents is complicated by issues of species selectivity. Figure 7 illustrates the effect of varying concentrations of compound 2 on the PT measured in the plasma of several different species. These results are representative of the general trend for this series, that rabbit plasma most closely resembles human plasma in its susceptibility to the anticoagulant action of these fXa inhibitors. However, a 2–10-fold decrease in sensitivity is observed when the same experiments are done in dog or rat plasma. Presumably, this variability reflects differences in the affinity of the inhibitors for the various forms of fXa. However, purified enzyme has not been isolated from animal plasmas to confirm this hypothesis.<sup>25</sup>

Our initial efforts to demonstrate the antithrombotic activity of these anticoagulants in small animals were attempted in the rat AV shunt model which was routinely used in our thrombin inhibitor program.<sup>26</sup> As depicted in Figure 8, a dose-dependent decrease in



**Figure 8.** Comparison of the antithrombotic potency in the arteriovenous (AV) shunt model of thrombosis in the rat of a thrombin inhibitor (D-1-Piq-Pro-ArgH) and fXa inhibitors. Drug was infused for 30 min. Blood was circulated through the shunt, and the thrombus was formed during the final 15 min of the infusion. ED<sub>50%</sub> (mg/kg/h) is the dose required under these conditions to reduce thrombus weight to 50% of the corresponding vehicle control and is calculated from the best-fit linear regression equation.

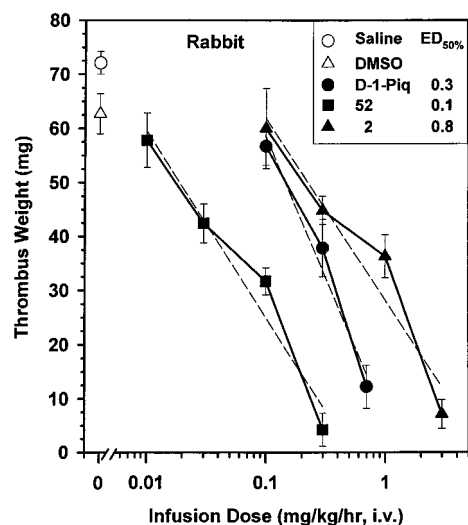
thrombus weight was achieved for both **2** and **52**. The ED<sub>50</sub> observed for compound **52** (1.1 mg/kg/h) was left-shifted 8-fold relative to that for compound **2** (9.3 mg/kg/h) reflecting the difference in fXa affinity for the compounds. However, since D-1-Piq-Pro-ArgH is not adversely affected by species selectivity in rat plasma, the thrombin inhibitor is significantly more potent in this model than either of the two fXa inhibitors.

To more effectively compare these fXa inhibitors with D-1-Piq-Pro-ArgH and related thrombin inhibitors, the AV shunt model was modified to run in rabbits where the anticoagulant activity of both series is similar to that observed in human plasma. The dose-response curves for compounds **2**, **52**, and D-1-Piq-Pro-ArgH in the rabbit AV shunt model are illustrated in Figure 9. As in the rat model, compound **52** was observed to be significantly more potent than compound **2** (ED<sub>50</sub> = 0.07 mg/kg/h vs 0.81 mg/Kg/h, 11-fold shift in the dose-response curve). However, based on the increased sensitivity of rabbit plasma to this series of fXa inhibitors, compound **52** was observed to be significantly more potent than the thrombin inhibitor D-Piq-Pro-ArgH, which showed almost identical activities in the rabbit (ED<sub>50</sub> = 0.27 mg/kg/h) relative to the rat (ED<sub>50</sub> = 0.30 mg/kg/h).

Thus, while both the rat and rabbit models produced similar differences in potency for the two fXa inhibitors **2** and **52**, they made significantly different predictions about the potency of the fXa inhibitors relative to thrombin inhibitors. These results underscore the importance of using species selectivity profiles to guide the selection of appropriate models for SAR development.

## Conclusion

We have demonstrated that the incorporation of an amidine into the *meta*-position of one of the side chains of dibenzamidobenzene derivatives related to **1** produces a significant increase in fXa affinity. By coupling structure-based inhibitor design with synthesis/biologi-



**Figure 9.** Comparison of the antithrombotic potency in the arteriovenous (AV) shunt model of thrombosis in the rabbit of a thrombin inhibitor (D-1-Piq-Pro-ArgH) and fXa inhibitors. Drug was infused for 30 min. Blood was circulated through the shunt, and the thrombus was formed during the final 15 min of the infusion. ED<sub>50%</sub> (mg/kg/h) is the dose required under these conditions to reduce thrombus weight to 50% of the corresponding vehicle control and is calculated from the best-fit linear regression equation.

cal evaluation, fXa affinity was increased by 3 orders of magnitude in two iterative steps. The SAR results provided support for a computational model in which the *meta*-substituted benzamidine occupies the S1 binding site and a *para*-substituted *tert*-butylphenyl group binds into the neighboring S4 site of fXa. This work also illustrates the benefits of obtaining structural data using surrogate proteins if such data is not available for the target protein.

This series of fXa inhibitors demonstrates high levels of selectivity for the inhibition of fXa relative to serine proteases such as thrombin and trypsin and particularly with respect to the fibrinolytic enzymes and aPC. Further, the fXa affinity of these inhibitors effectively translates into potent anticoagulant activity *in vitro* and antithrombotic activity *in vivo*, providing additional support for the validation of fXa as a target for the treatment of thrombotic disease.

## Experimental Section

**Chemistry.** Procedures for the preparation of all final products are presented below along with representative procedures for all methods used in the preparation of intermediates. The additional intermediates not specifically presented in this section can be found in the Supporting Information.

All reactions were run under an atmosphere of dry nitrogen unless noted. All solvents and reagents were used as acquired from commercial sources without purification. Nuclear magnetic resonance spectra were recorded at 300 MHz on a GE QE-300 spectrophotometer in the solvent indicated. Chemical shifts are reported in parts per million relative to tetramethylsilane. Infrared spectra were recorded on a Nicolet DX10 FT-IR spectrometer. Melting points were recorded on a Thomas-Hoover melting point apparatus and are uncorrected. Mass spectra were recorded on the following instruments, using the stated ionization methods: VG Analytical 70SE mass spectrometer, field-desorption (FD); VG Analytical ZAB2-SE instrument, fast atom bombardment (FAB); Sciex API 100 mass spectrometer, electrospray ionization (ESI). Elemental analyses were performed by the Physical Chemistry Department

at Lilly Research Laboratories on a Control Equipment Corp. 440 elemental analyzer and are within 0.4% of theory unless otherwise noted. Analytical HPLC were performed on a Hitachi L-6200 instrument over a Vydac C<sub>18</sub> analytical column, eluting with mixtures of acetonitrile in water, buffered with 0.1% TFA.

**N<sup>1</sup>-(3-(Aminoiminomethyl)benzoyl)-N<sup>2</sup>-(4-methoxybenzoyl)-1,2-benzenediamine Hydrochloride (2).** Hydrogen sulfide was bubbled through a solution of compound **21** (0.5 g, 1.35 mmol) in triethylamine (5 mL) and pyridine (50 mL) for 5 min, and then the reaction vessel was sealed and allowed to stand for 48 h. The solvents were then removed in vacuo and the residue was dissolved in ethyl acetate and washed twice with brine. The organic phase was dried with MgSO<sub>4</sub>, filtered, and concentrated. The residue was then dissolved in acetone (100 mL), iodomethane (25 mL, 641.7 mmol) was added, and the vessel was heated to reflux for 2 h, cooled, and the solvent removed in vacuo. The residue was then dissolved in methanol (100 mL) and ammonium acetate (0.15 g, 5.4 mmol) was added. This solution was heated to reflux for 12 h, cooled and concentrated. The resulting residue was dissolved in THF (20 mL) and di-*tert*-butyl dicarbonate (0.87 g, 4 mmol) was added, followed by a solution of K<sub>2</sub>CO<sub>3</sub> (0.93 g, 6.75 mmol) in water (10 mL). After 2 h, the reaction was concentrated. The residue was then dissolved in a minimal amount of chloroform and chromatographed (30% ethyl acetate/hexanes to ethyl acetate). This material was dissolved in trifluoroacetic acid, stirred for 2 h, and concentrated. To the residue was added 1 N HCl, and the mixture was stirred vigorously, filtered and vacuum-dried to give the title compound as a white solid (220 mg, 42%): <sup>1</sup>H NMR (300 MHz, DMSO-*d*<sub>6</sub>) δ 3.83 (s, 3H), 7.05 (d, *J* = 8.8 Hz, 2H), 7.25–7.35 (m, 2H), 7.65–7.75 (m, 2H), 7.78 (t, *J* = 7.8 Hz, 1H), 8.00 (m, 1H), 8.03 (d, *J* = 8.8 Hz, 2H), 8.30 (d, *J* = 7.8 Hz, 1H), 8.49 (s, 1H), 9.22 (s, 2H), 9.51 (s, 2H), 10.10 (s, 1H), 10.58 (s, 1H); MS(FD) *m/e* 389.1 (MH<sup>+</sup>). Anal. (C<sub>22</sub>H<sub>20</sub>N<sub>4</sub>O<sub>3</sub>·1.0HCl·1.2H<sub>2</sub>O) C, H, N.

**N<sup>1</sup>-(4-(Aminoiminomethyl)benzoyl)-N<sup>2</sup>-(4-methoxybenzoyl)-1,2-benzenediamine Hydrochloride (3).** Following the procedure used in the preparation of compound **2**, **3** was prepared from compound **22**: 26% yield; <sup>1</sup>H NMR (300 MHz, DMSO-*d*<sub>6</sub>) δ 3.83 (s, 3H), 7.05 (d, *J* = 8.8 Hz, 2H), 7.25–7.35 (m, 2H), 7.60–7.70 (m, 2H), 7.95 (d, *J* = 8.8 Hz, 2H), 8.01 (d, *J* = 8.8 Hz, 2H), 8.17 (d, *J* = 8.8 Hz, 2H), 9.20 (s, 2H), 9.48 (s, 2H), 10.13 (s, 1H), 10.43 (s, 1H); MS(FD) *m/e* 389.1 (MH<sup>+</sup>). Anal. (C<sub>22</sub>H<sub>20</sub>N<sub>4</sub>O<sub>3</sub>·1.1HCl·0.5H<sub>2</sub>O) C, H, N.

**N<sup>1</sup>,N<sup>2</sup>-Bis(4-methoxybenzoyl)-4-aminoiminomethyl-1,2-benzenediamine Hydrochloride (4).** To a stirring solution of compound **36** (0.5 g, 1.2 mmol) in tetrahydrofuran (5 mL), ethanol (50 mL) and water (25 mL) was added 1 N HCl (1.5 mL) followed by 10% Pd/C (0.25 g). The vessel was placed under vacuum and the atmosphere replaced with hydrogen. After stirring under hydrogen for 24 h, Celite was added and the mixture was filtered through a pad of Celite. The filtrate was concentrated in vacuo and the residue was precipitated from methanol with ether, filtered and dried to give 0.18 g (35% yield) of off-white solid: <sup>1</sup>H NMR (300 MHz, DMSO-*d*<sub>6</sub>) δ 3.85 (s, 6H), 7.08 (br d, *J* = 6.6 Hz, 4H), 7.78 (d, *J* = 8.5 Hz, 1H), 7.99 (d, *J* = 8.5 Hz, 1H), 8.10–8.20 (m, 5H), 9.24 (s, 2H), 9.45 (s, 2H), 10.61 (s, 1H), 10.67 (s, 1H); MS(FD) *m/e* 419 (MH<sup>+</sup>). Anal. (C<sub>23</sub>H<sub>22</sub>N<sub>4</sub>O<sub>4</sub>·1.1HCl·1.0H<sub>2</sub>O) C, H, N.

**2-Nitro-4-(*tert*-butyldimethylsilyloxy)aniline (6).** To a mixture of 4-amino-3-nitrophenol (10.07 g, 65.3 mmol) and *N,N*-dimethylformamide (20 mL) was added imidazole (11.15 g, 163.8 mmol) followed by *tert*-butyldimethylsilyl chloride (11.82 g, 78.4 mmol) in several portions. After 5 h, the reaction was diluted with ethyl acetate (150 mL) and washed with water (5 × 20 mL). The organic layer was dried with MgSO<sub>4</sub>, filtered, and concentrated. The residue was chromatographed over silica gel, eluting with a gradient of 10% ethyl acetate/hexanes to 20% ethyl acetate/hexanes to give the title compound as a solid (17.06 g, 97%): <sup>1</sup>H NMR (300 MHz, CDCl<sub>3</sub>) δ 0.19 (s, 6H), 0.97 (s, 9H), 6.70 (d, *J* = 9.0 Hz, 1H), 6.95 (d, *J* = 3.0 Hz, 1H), 7.56 (d, *J* = 2.7 Hz, 1H); IR (CHCl<sub>3</sub>) 3399, 2932,

1519, 1242, 866 cm<sup>-1</sup>; MS(FD) *m/e* 268.2; mp 80–83 °C. Anal. (C<sub>12</sub>H<sub>20</sub>N<sub>2</sub>O<sub>3</sub>Si) C, H, N.

**3,4-Diaminobenzonitrile (8).** To a stirring solution of 3-nitro-4-aminobenzonitrile (4 g, 24.5 mmol) in THF (350 mL) under nitrogen was added 10% Pd/C (2 g). The flask was placed under vacuum and the atmosphere was replaced by hydrogen. After stirring overnight, the mixture was filtered through Celite and concentrated to a small volume in vacuo. The solution was triturated with diethyl ether and the precipitate was filtered and dried in vacuo to give 1.89 g (58%) of the title compound: <sup>1</sup>H NMR (300 MHz, DMSO-*d*<sub>6</sub>) δ 3.40 (br s, 2H), 3.84 (br s, 2H), 6.68 (d, *J* = 8.1 Hz, 1H), 6.94 (d, *J* = 1.5, Hz, 1H), 7.04 (dd, *J* = 1.5, 8.1 Hz, 1H); MS(ESI) *m/e* 133.05 (MH<sup>+</sup>).

**N-(4-Methoxybenzoyl)-2-nitroaniline (9).** To a stirring solution of 2-nitroaniline (7.5 g, 54.3 mmol) in pyridine (50 mL) was added 4-anisoyl chloride (8.5 mL, 59.7 mmol). After 30 min, the solvent was removed in vacuo and the residue was partitioned between ethyl acetate and water. The organic phase was washed twice with 1 M citric acid, twice with water, and twice with brine. The organic phase was then dried with MgSO<sub>4</sub>, filtered and concentrated to give 14.6 g (98%) of a light yellow solid: <sup>1</sup>H NMR (300 MHz, DMSO-*d*<sub>6</sub>) δ 3.85 (s, 3H), 7.11 (d, *J* = 9.0 Hz, 2H), 7.40 (dt, *J* = 1.5, 7.0 Hz, 1H), 7.71–7.84 (m, 2H), 7.95 (d, *J* = 9.0 Hz, 2H), 8.01 (dd, *J* = 1.3, 8.3 Hz, 1H), 10.63 (s, 1H); MS(FD) *m/e* 272.0. Anal. (C<sub>14</sub>H<sub>12</sub>N<sub>2</sub>O<sub>4</sub>) C, H, N.

**N-(3-Cyanobenzoyl)-2-nitro-4-(*tert*-butyldimethylsilyloxy)aniline (12).** To a stirring suspension of **6** (10.01 g, 37.30 mmol) in dichloromethane (400 mL) at 0 °C was added pyridine (3.4 mL, 42.0 mmol) followed by the 3-cyanobenzoyl chloride (8.65 g, 52.2 mmol). The reaction was allowed to warm to room temperature and stirred for 1 h. The reaction was diluted with dichloromethane (800 mL) and washed with saturated aqueous NH<sub>4</sub>Cl (2 × 200 mL). The organic layer was MgSO<sub>4</sub> dried, filtered, and concentrated. The residue was chromatographed (20% EtOAc/hexanes) to give the title compound as a solid (13.94 g, 94%): <sup>1</sup>H NMR (300 MHz, CDCl<sub>3</sub>) δ 0.27 (s, 6H), 1.02 (s, 9H), 7.27 (s, 1H), 7.70 (m, 2H), 7.90 (d, *J* = 7.8 Hz, 1H), 8.16 (d, *J* = 1.2 Hz, 1H), 8.30 (s, 1H), 8.79 (d, *J* = 9.3 Hz, 1H), 11.15 (br s, 1H); IR (CHCl<sub>3</sub>) 2932, 1689, 1508, 1289, 863 cm<sup>-1</sup>; MS(FD) *m/e* 397.0. Anal. (C<sub>20</sub>H<sub>23</sub>N<sub>3</sub>O<sub>4</sub>Si) C, H, N.

**N<sup>1</sup>-(4-Methoxybenzoyl)-1,2-benzenediamine (13).** To a stirring solution of **9** (25 g, 91.8 mmol) in ethyl acetate (300 mL) under nitrogen was added 10% Pd/C (12 g). The flask was placed under vacuum and then the atmosphere was replaced with hydrogen (balloon) and allowed to stir overnight. Celite was added and the solution was filtered through a pad of Celite. The solvent was then removed in vacuo to give 9.5 g (43%) of white solid. The catalyst/Celite mixture was washed with tetrahydrofuran, filtered and concentrated in vacuo. The resulting solid was triturated from ether to give a second crop (9.9 g, 45%) of white solid: <sup>1</sup>H NMR (300 MHz, DMSO-*d*<sub>6</sub>) δ 3.83 (s, 3H), 4.86 (br s, 2H), 6.59 (dt, *J* = 1.5, 8.0 Hz, 1H), 6.78 (dd, *J* = 1.3, 8.0 Hz, 1H), 6.97 (dt, *J* = 1.3, 8.0 Hz, 1H), 7.04 (d, *J* = 8.8 Hz, 2H), 7.15 (dd, *J* = 1.3, 8.0 Hz, 1H), 7.97 (d, *J* = 8.8 Hz, 2H), 9.54 (s, 1H); MS(FD) *m/e* 242. Anal. (C<sub>14</sub>H<sub>14</sub>N<sub>2</sub>O<sub>2</sub>) C, H, N.

**N<sup>1</sup>-(4-*tert*-Butylbenzoyl)-4-methoxycarbonyl-1,2-benzenediamine (17).** To a stirring solution of 4-methoxycarbonyl-1,2-benzenediamine (**7**) (8.5 g, 51 mmol) and pyridine (4.1 mL, 51 mmol) in acetonitrile (200 mL) was added, over about 15 min via an addition funnel, a solution of 4-*tert*-butylbenzoyl chloride (10 g, 51 mmol) in acetonitrile (50 mL). After 3 h, the solution was concentrated in vacuo to a volume of about 50 mL, diluted with ethyl acetate (300 mL) and washed twice with 1 M citric acid, once with brine, twice with saturated aqueous NaHCO<sub>3</sub>, and once with brine. The organic phase was then dried with MgSO<sub>4</sub>, filtered, partially concentrated in vacuo and then allowed to stand for 72 h. The solid was then filtered and dried to give 8.2 g (49%) of the title compound. A second crop of 2.6 g (16%) was isolated from the mother liquor: <sup>1</sup>H NMR (300 MHz, DMSO-*d*<sub>6</sub>) δ 1.32 (s, 9H), 3.77 (s, 3H), 5.83 (br s, 2H), 6.79 (d, *J* = 8.5 Hz, 1H), 7.53 (d, *J* = 8.3 Hz, 2H), 7.62

(dd,  $J = 2.0, 8.5$  Hz, 1H), 7.83 (d,  $J = 2.0$  Hz, 1H), 7.95 (d,  $J = 8.3$  Hz, 2H), 9.60 (s, 1H); MS(FD)  $m/e$  326.2. Anal. (C<sub>19</sub>H<sub>22</sub>N<sub>2</sub>O<sub>3</sub>) C, H, N.

***N*-(3-Cyanobenzoyl)-*N*'-(4-isopropylbenzoyl)-4-(*tert*-butyldimethylsilyloxy)-1,2-benzenediamine (25).** A mixture of compound **12** (5.00 g, 12.6 mmol), 10% Pd/C (2.5 g), ethanol (160 mL), and tetrahydrofuran (160 mL) was placed under an atmosphere of hydrogen (balloon) with stirring for 12 h. The mixture was filtered through diatomaceous earth with hot methanolic washes. The filtrate was concentrated and chromatographed over silica gel, eluting with a gradient of 20% to 30% ethyl acetate in hexanes. The fractions containing compound **16** (contaminated) were combined and concentrated in vacuo to give 2.72 g of yellow solid (MS(ESI)  $m/e$  367.9).

The solid was dissolved in dichloromethane (45 mL) and cooled to 0 °C. To this solution was added pyridine (0.65 mL, 8.0 mmol) followed by a solution of 4-isopropylbenzoyl chloride (10.1 mmol) in dichloromethane (90 mL). The reaction was allowed to warm to room temperature and stirred for 10 min. The mixture was diluted with dichloromethane (200 mL) and washed with saturated aqueous NH<sub>4</sub>Cl (2 × 50 mL). The organic layer was separated and dried with MgSO<sub>4</sub> filtered, and concentrated. The residue was chromatographed over silica gel, eluting with 10% to 20% ethyl acetate in hexanes. The product containing fractions were combined and concentrated to give 3.04 g (83%) of the title compound: <sup>1</sup>H NMR (300 MHz, CDCl<sub>3</sub>)  $\delta$  0.16 (s, 6H), 0.95 (s, 9H), 1.29 (s, 3H), 1.31 (s, 3H), 3.00 (m, 1H), 6.68 (d,  $J = 9.0$  Hz, 1H), 6.86 (s, 1H), 7.38 (d,  $J = 8.1$  Hz, 2H), 7.50 (d,  $J = 9.0$  Hz, 1H), 7.61 (m, 1H), 7.81 (d,  $J = 6.3$  Hz, 1H), 7.89 (d,  $J = 7.1$  Hz, 2H), 8.16 (d,  $J = 9.3$  Hz, 1H), 8.29 (s, 1H), 8.58 (br s, 1H), 9.40 (br s, 1H); IR (CHCl<sub>3</sub>) 2962, 1656, 1610, 1513, 1473, 1295 cm<sup>-1</sup>; MS(FD)  $m/e$  513.1. Anal. (C<sub>30</sub>H<sub>35</sub>N<sub>3</sub>O<sub>3</sub>Si) C, H, N.

***N*-(3-Cyanobenzoyl)-*N*'-(4-isopropylbenzoyl)-4-hydroxy-1,2-benzenediamine (29).** To a mixture of compound **25** (1.57 g, 3.05 mmol) and tetrahydrofuran (30 mL) at 0 °C was added a 1.0 M solution of tetra-*n*-butylammonium fluoride in tetrahydrofuran (3.1 mL, 3.1 mmol). After 1 h, the reaction was quenched with water (35 mL) and extracted with diethyl ether (2 × 200 mL). The combined organic layers were dried with MgSO<sub>4</sub>, filtered, and concentrated. The residue was chromatographed over silica gel, eluting with 1:1 ethyl acetate/hexanes to give the title compound as a solid (1.10 g, 91%): <sup>1</sup>H NMR (300 MHz, DMSO-*d*<sub>6</sub>)  $\delta$  1.15 (s, 3H), 1.17 (s, 3H), 2.90 (m, 1H), 6.63 (d,  $J = 9.0$  Hz, 1H), 7.34–7.21 (m, 4H), 7.70 (m, 1H), 7.79 (d,  $J = 8.1$  Hz, 2H), 8.01 (d,  $J = 7.2$  Hz, 1H), 8.18 (d,  $J = 7.5$  Hz, 1H), 8.31 (s, 1H), 9.56 (s, 1H), 9.70 (s, 1H), 10.02 (s, 1H); IR (KBr) 3277, 1629, 1600, 1535, 1478, 1299 cm<sup>-1</sup>; MS(FD)  $m/e$  399.1. Anal. (C<sub>24</sub>H<sub>21</sub>N<sub>3</sub>O<sub>3</sub>) C, H, N.

***N*-(3-Cyanobenzoyl)-*N*'-(4-isopropylbenzoyl)-4-benzoyloxycarbonylmethoxy-1,2-benzenediamine (30).** To a mixture of compound **29** (502 mg, 1.26 mmol), acetone (15 mL), and potassium carbonate (216 mg, 1.56 mmol) was added benzyl 2-bromoacetate (0.4 mL, 2.52 mmol). After stirring overnight, the reaction was concentrated and the residue was chromatographed (100% dichloromethane to 10% ethyl acetate in dichloromethane) to give the title compound as a solid (532 mg, 77%): <sup>1</sup>H NMR (300 MHz, CDCl<sub>3</sub>)  $\delta$  1.28 (s, 3H), 1.30 (s, 3H), 3.00 (m, 1H), 4.50 (s, 2H), 5.22 (s, 2H), 6.71 (d,  $J = 9.3$  Hz, 1H), 6.93 (s, 1H), 7.31 (m, 7H), 7.54 (d,  $J = 21$  Hz, 1H), 7.60 (t,  $J = 7.8$  Hz, 1H), 7.78 (d,  $J = 8.7$  Hz, 1H), 7.89 (d,  $J = 8.1$  Hz, 2H), 8.19 (d,  $J = 8.1$  Hz, 1H), 8.30 (s, 1H), 8.74 (br s, 1H), 9.48 (br s, 1H); IR (CHCl<sub>3</sub>) 2965, 1759, 1654, 1610, 1514, 1175 cm<sup>-1</sup>; MS(FD)  $m/e$  547. Anal. (C<sub>33</sub>H<sub>29</sub>N<sub>3</sub>O<sub>5</sub>) C, H, N.

***N*-(3-Cyanobenzoyl)-*N*'-(4-*tert*-butylbenzoyl)-4-benzoyloxycarbonyl-1,2-benzenediamine (32).** To a solution of compound **26** (5 g, 11 mmol) in tetrahydrofuran (100 mL) was added methanol (30 mL), followed by a solution of LiOH·H<sub>2</sub>O (1.4 g, 33 mmol) in water (30 mL). After stirring overnight, more LiOH·H<sub>2</sub>O (0.67 g, 16 mmol) in water (5 mL) was added. After stirring for another 24 h, the pH was adjusted to 3 with concentrated HCl and the mixture was concentrated in vacuo. The residue was partitioned between ethyl acetate and water. The organic layer was washed with 1 N HCl, brine (2×),

MgSO<sub>4</sub> dried, and concentrated. A portion of the residue (4 g, 9.06 mmol) was dissolved in *N,N*-dimethylformamide (25 mL). Benzyl bromide (1.06 g, 6.2 mmol) was added, followed by K<sub>2</sub>CO<sub>3</sub> (1.6 g, 11.4 mmol). After 3 h, the reaction was concentrated and the residue was dissolved in ethyl acetate and washed with saturated aqueous NaHCO<sub>3</sub> followed by brine. The organic layer was MgSO<sub>4</sub> dried, filtered and 5 g of silica gel was added. This mixture was concentrated to a dry pack, loaded onto a silica gel column and chromatographed (10% ethyl acetate/hexanes to 30% ethyl acetate/hexanes) to give the title compound as a white solid (3.3 g, 65%): <sup>1</sup>H NMR (300 MHz, DMSO-*d*<sub>6</sub>)  $\delta$  1.30 (s, 9H), 5.39 (s, 2H), 7.35–7.60 (m, 7H), 7.76 (t,  $J = 8.0$  Hz, 1H), 7.85–7.95 (m, 4H), 8.08 (d,  $J = 8.0$  Hz, 1H), 8.24 (d,  $J =$  Hz, 1H), 8.33 (s, 1H), 8.38 (s, 1H), 10.07 (s, 1H), 10.37 (s, 1H); MS(FD)  $m/e$  531.0. Anal. (C<sub>33</sub>H<sub>29</sub>N<sub>3</sub>O<sub>4</sub>) C, H, N.

***N,N*'-Bis(4-methoxybenzoyl)-4-(amino(hydroxyimino)-methyl)-1,2-benzenediamine (34).** To a stirring solution of compound **28** (0.75 g, 1.87 mmol) in ethanol (100 mL) was added hydroxylamine hydrochloride (0.13 g, 1.87 mmol) followed by *N,N*-diisopropylethylamine (0.3 mL, 1.87 mmol). The solution was heated to reflux and after 6 h, the solution was concentrated. The residue was dissolved in ethyl acetate and washed with brine, then dried with MgSO<sub>4</sub> and filtered. The solution was then allowed to stand and then filtered to give 0.77 g (95%) of a white solid: <sup>1</sup>H NMR (300 MHz, DMSO-*d*<sub>6</sub>)  $\delta$  3.83 (s, 6H), 5.84 (s, 2H), 7.07 (d,  $J = 7.7$  Hz, 4H), 7.57 (dd,  $J = 1.8, 8.5$  Hz, 1H), 7.67 (d,  $J = 8.5$  Hz, 1H), 7.9–8.1 (m, 5H), 9.67 (s, 1H), 10.08 (s, 1H), 10.14 (s, 1H); MS(FD)  $m/e$  434.1. Anal. (C<sub>23</sub>H<sub>22</sub>N<sub>4</sub>O<sub>5</sub>·1.1H<sub>2</sub>O) C, H, N.

***N*-(3-(Aminoiminomethyl)benzoyl)-*N*'-(4-*tert*-butylbenzoyl)-1,2-benzenediamine Hydrochloride (44).** Following the procedure described in the preparation of compound **4**, **44** was prepared from compound **35**: 76% yield; <sup>1</sup>H NMR (300 MHz, DMSO-*d*<sub>6</sub>)  $\delta$  1.32 (s, 9H), 7.28–7.32 (m, 2H), 7.52 (d,  $J = 10.2$  Hz, 2H), 7.62–7.67 (m, 1H), 7.67–7.71 (m, 1H), 7.77 (t,  $J = 9.3$  Hz, 1H), 7.96 (d,  $J = 10.2$  Hz, 2H), 8.00 (d,  $J = 10.8$  Hz, 1H), 8.30 (d,  $J = 9.3$  Hz, 1H), 8.49 (s, 1H), 9.20 (s, 1H), 9.49 (s, 1H), 10.13 (s, 1H), 10.56 (s, 1H); MS(FD)  $m/e$  415; mp 196–198 °C. Anal. (C<sub>25</sub>H<sub>26</sub>N<sub>4</sub>O<sub>2</sub>·1.0HCl·0.75H<sub>2</sub>O) C, H, N.

***N*-(4-(Aminoiminomethyl)benzoyl)-*N*'-(4-*tert*-butylbenzoyl)-1,2-benzenediamine Hydrochloride (45).** Following the procedure described for the synthesis of compound **4**, **45** was prepared from compound **36**: 77% yield; <sup>1</sup>H NMR (300 MHz, DMSO-*d*<sub>6</sub>)  $\delta$  1.30 (s, 9H), 7.27–7.33 (m, 2H), 7.53 (d,  $J = 8.5$  Hz, 2H), 7.62–7.70 (m, 2H), 7.95 (d,  $J = 8.5$  Hz, 4H), 8.19 (d,  $J = 8.3$  Hz, 2H), 9.20 (br s, 2H), 9.47 (br s, 2H), 10.19 (s, 1H), 10.42 (s, 1H); MS(FD)  $m/e$  414.9. Anal. (C<sub>25</sub>H<sub>26</sub>N<sub>4</sub>O<sub>2</sub>·1.2HCl·1.1H<sub>2</sub>O) C, H, N.

***N*-(3-(Aminoiminomethyl)benzoyl)-*N*'-(4-ethoxybenzoyl)-1,2-benzenediamine Hydrochloride (46).** Following the procedure described for the preparation of compound **4**, **46** was prepared from compound **37**: 21% yield; 96% pure by analytical HPLC, gradient = 5% to 50% acetonitrile, 1%/min,  $t_R = 28.35$  min; <sup>1</sup>H NMR (300 MHz, DMSO-*d*<sub>6</sub>)  $\delta$  1.31 (t,  $J = 7.0$  Hz, 3H), 4.07 (q, 2H), 7.01 (d,  $J = 7.0$  Hz, 2H), 7.20 (m, 2H), 7.60 (m, 2H), 7.65 (t,  $J = 7.8$  Hz, 1H), 8.00 (m, 3H), 8.29 (d,  $J = 7.8$  Hz, 1H), 8.54 (s, 1H), 9.33 (s, 2H), 9.54 (s, 2H), 10.14 (s, 1H), 10.72 (s, 1H); MS(FD)  $m/e$  402; mp 163–165 °C.

***N*-(3-(Aminoiminomethyl)benzoyl)-*N*'-(4-isopropylbenzoyl)-1,2-benzenediamine Hydrochloride (47).** Following the procedure described for the synthesis of compound **4**, **47** was prepared from compound **38**: 63% yield; <sup>1</sup>H NMR (300 MHz, DMSO-*d*<sub>6</sub>)  $\delta$  1.20 (d, 6H), 2.95 (sept, 1H), 7.25–7.35 (m, 2H), 7.40 (d, 2H), 7.60–7.70 (m, 2H), 7.75 (t, 1H), 7.95 (d, 2H), 8.00 (d, 1H), 8.40 (d, 1H), 8.50 (s, 1H), 9.25 (br s, 2H), 9.50 (br s, 2H), 10.15 (s, 1H), 10.60 (s, 1H); MS(FD)  $m/e$  401.1; mp 227–229 °C. Anal. (C<sub>24</sub>H<sub>25</sub>N<sub>4</sub>O<sub>2</sub>·HCl·1.5H<sub>2</sub>O) C, H, N.

***N*-(3-(Aminoiminomethyl)benzoyl)-*N*'-(4-isopropylbenzoyl)-4-hydroxy-1,2-benzenediamine Hydrochloride (48).** Following the procedure described for the preparation of compound **4**, **48** was prepared from compound **39**: 62% yield; <sup>1</sup>H NMR (300 MHz, DMSO-*d*<sub>6</sub>)  $\delta$  1.17 (s, 3H), 1.19 (s, 3H), 2.90

(m, 1H), 6.65 (d,  $J = 8.7$  Hz, 1H), 7.28 (m, 4H), 7.73 (t,  $J = 7.8$  Hz, 1H), 7.86 (d,  $J = 8.1$  Hz, 2H), 7.94 (d,  $J = 7.2$  Hz, 1H), 8.23 (d,  $J = 7.5$  Hz, 1H), 8.42 (s, 1H), 9.14 (s, 2H), 9.45 (s, 2H), 9.89 (s, 1H), 10.27 (s, 1H); MS(FD)  $m/e$  399.2 (M - OH)<sup>+</sup>. Anal. (C<sub>24</sub>H<sub>24</sub>N<sub>4</sub>O<sub>3</sub>·1.5HCl·1.75H<sub>2</sub>O) C, H, N; 5.81, calcd 5.32.

**N<sup>1</sup>-(3-(Aminoiminomethyl)benzoyl)-N<sup>2</sup>-(4-isopropylbenzoyl)-4-carboxymethoxy-1,2-benzenediamine Hydrochloride (49).** Following the procedure used in the synthesis of compound **4**, **49** was prepared from compound **40**: 62% yield; <sup>1</sup>H NMR (300 MHz, DMSO-*d*<sub>6</sub>) δ 1.17 (s, 3H), 1.19 (s, 3H), 2.92 (m, 1H), 4.68 (s, 2H), 6.84 (d,  $J = 9.0$  Hz, 2H), 7.34 (d,  $J = 8.4$  Hz, 2H), 7.44 (d,  $J = 8.7$  Hz, 1H), 7.74 (t,  $J = 7.8$  Hz, 1H), 7.89 (d,  $J = 7.8$  Hz, 2H), 7.96 (d,  $J = 8.4$  Hz, 1H), 8.26 (d,  $J = 7.8$  Hz, 1H), 8.42 (s, 1H), 9.15 (s, 2H), 9.45 (s, 2H), 10.01 (s, 1H), 10.36 (s, 1H); MS(FD)  $m/e$  474. Anal. (C<sub>26</sub>H<sub>26</sub>N<sub>4</sub>O<sub>5</sub>·2.0HCl·1.0H<sub>2</sub>O) C, H, N.

**N<sup>1</sup>-(3-(Aminoiminomethyl)benzoyl)-N<sup>2</sup>-(4-isopropylbenzoyl)-4-ethoxycarbonylmethoxy-1,2-benzenediamine Hydrochloride (50).** Following the procedure described for the preparation of compound **4**, **50** was prepared from compound **41**: 65% yield; <sup>1</sup>H NMR (300 MHz, DMSO-*d*<sub>6</sub>) δ 1.03 (t,  $J = 7.1$  Hz, 3H), 1.17 (s, 3H), 1.19 (s, 3H), 2.92 (m, 1H), 4.17 (q,  $J = 6.9$  Hz, 2H), 4.78 (s, 2H), 6.83 (d,  $J = 9.0$  Hz, 1H), 7.34 (d,  $J = 7.8$  Hz, 3H), 7.45 (d,  $J = 8.7$  Hz, 1H), 7.74 (t,  $J = 7.8$  Hz, 1H), 7.88 (d,  $J = 7.8$  Hz, 2H), 7.95 (d,  $J = 8.4$  Hz, 1H), 8.24 (d,  $J = 7.8$  Hz, 1H), 8.42 (s, 1H), 9.13 (s, 2H), 9.45 (s, 2H), 9.99 (s, 1H), 10.34 (s, 1H); MS(FD)  $m/e$  503. Anal. (C<sub>28</sub>H<sub>30</sub>N<sub>4</sub>O<sub>5</sub>·1.0HCl·1.0H<sub>2</sub>O) C, H, N.

**N<sup>1</sup>-(3-(Aminoiminomethyl)benzoyl)-N<sup>2</sup>-(4-*tert*-butylbenzoyl)-4-carboxy-1,2-benzenediamine Hydrochloride (51).** Following the procedure used in the preparation of compound **4**, **51** was prepared from compound **42**: 90% yield; <sup>1</sup>H NMR (300 MHz, DMSO-*d*<sub>6</sub>) δ 1.30 (s, 9H), 7.53 (d,  $J = 8.3$  Hz, 2H), 7.78 (t,  $J = 8.0$  Hz, 1H), 7.85 (s, 2H), 8.00 (d,  $J = 8.3$  Hz, 2H), 8.01 (m, 1H), 8.26 (s, 1H), 8.31 (d,  $J = 8.0$  Hz, 1H), 8.51 (s, 1H), 9.22 (s, 2H), 9.50 (s, 2H), 10.30 (s, 1H), 10.72 (s, 1H), 13.03 (br s, 1H); MS(FD)  $m/e$  459. Anal. (C<sub>26</sub>H<sub>26</sub>N<sub>4</sub>O<sub>4</sub>·1.15HCl·1.0H<sub>2</sub>O) C, H, N.

**N<sup>1</sup>-(3-(Aminoiminomethyl)benzoyl)-N<sup>2</sup>-(4-*tert*-butylbenzoyl)-5-carboxy-1,2-benzenediamine Hydrochloride (52).** Following the procedure used in the synthesis of compound **4**, **52** was prepared from compound **43**: 83% yield; <sup>1</sup>H NMR (300 MHz, DMSO-*d*<sub>6</sub>) δ 1.30 (s, 9H), 7.47 (d,  $J = 8.5$  Hz, 2H), 7.75–8.05 (m, 6H), 8.20 (s, 1H), 8.35 (d,  $J = 7.8$  Hz, 1H), 8.55 (s, 1H), 9.25 (s, 2H), 9.53 (s, 2H), 10.25 (s, 1H), 10.75 (s, 1H), 12.95 (br s, 1H); MS(FD)  $m/e$  441 (M - OH)<sup>+</sup>. Anal. (C<sub>26</sub>H<sub>26</sub>N<sub>4</sub>O<sub>4</sub>·1.1HCl·0.5H<sub>2</sub>O) C, H, N.

**N-(4-Methoxyphenyl)-2-aminobenzamide (54).** A mixture of compound **53** (4.894 g, 30 mmol), 4-methoxyaniline (3.695 g, 30 mmol) and toluene (60 mL) was heated to reflux for 5 h. After cooling, the reaction was filtered. The solid was triturated with dichloromethane (500 mL). This supernatant was combined with the above filtrate and concentrated. The residue was dissolved in dichloromethane, decolorized with activated charcoal and crystallized from dichloromethane/hexanes to give the title compound as a white solid (5.3 g, 73%); <sup>1</sup>H NMR (300 MHz, CDCl<sub>3</sub>) δ 3.81 (s, 3H), 5.50 (br s, 2H), 6.65–6.75 (m, 2H), 6.91 (d,  $J = 9.0$  Hz, 2H), 7.20–7.30 (m, 1H), 7.45–7.50 (m, 3H), 7.65 (br s, 1H); MS(FD)  $m/e$  242; mp 116–117 °C. Anal. (C<sub>14</sub>H<sub>14</sub>N<sub>2</sub>O<sub>2</sub>) C, H, N.

**N-(4-Methoxyphenyl)-2-(3-(aminoiminomethyl)benzoyl)aminobenzamide Hydrochloride (57).** Following the procedure described for the synthesis of compound **4**, **57** was prepared from compound **56**: 54% yield; <sup>1</sup>H NMR (300 MHz, DMSO-*d*<sub>6</sub>) δ 3.74 (s, 3H), 6.93 (d,  $J = 8.8$  Hz, 2H), 7.32 (t,  $J = 7.5$  Hz, 1H), 7.55–7.65 (m, 3H), 7.82 (t,  $J = 7.8$  Hz, 1H), 7.94 (d,  $J = 7.3$  Hz, 1H), 8.03 (d,  $J = 8.0$  Hz, 1H), 8.20 (d,  $J = 8.3$  Hz, 1H), 8.30–8.40 (m, 2H), 9.33 (s, 2H), 9.57 (s, 2H), 10.49 (s, 1H), 11.85 (s, 1H); MS(FD)  $m/e$  388.1; mp 163–167 °C. Anal. (C<sub>22</sub>H<sub>21</sub>N<sub>4</sub>O<sub>3</sub>·1.5HCl·1.5H<sub>2</sub>O) C, H, N.

**N-(3-(Aminoiminomethyl)phenyl)-2-(4-*tert*-butylbenzoyl)aminobenzamide Hydrochloride (62).** Following the procedure used in the preparation of compound **4**, **62** was prepared from compound **61**: 66% yield; <sup>1</sup>H NMR (300 MHz,

DMSO-*d*<sub>6</sub>) δ 1.29 (s, 9H), 7.30 (t,  $J = 7.2$  Hz, 1H), 7.57 (m, 5H), 7.83 (d,  $J = 7.8$  Hz, 2H), 7.89 (d,  $J = 7.5$  Hz, 1H), 7.94 (d,  $J = 8.1$  Hz, 1H), 8.17 (s, 1H), 8.36 (d,  $J = 8.1$  Hz, 1H), 9.01 (s, 2H), 9.35 (s, 2H), 10.85 (s, 1H), 11.42 (s, 1H); IR (CHCl<sub>3</sub>) 1528, 1656, 1676, 2968 cm<sup>-1</sup>; MS(FD)  $m/e$  415.3. Anal. (C<sub>25</sub>H<sub>27</sub>N<sub>4</sub>O<sub>2</sub>·HCl·1.5H<sub>2</sub>O) C, H, N.

**3-(4-*tert*-Butylbenzoylamino)thiophene-2-carboxylic Acid (65).** A mixture of compound **64** (9.67 g, 30 mmol), dioxane (75 mL) and 2 M sodium hydroxide (75 mL) was stirred for 16 h. The reaction was acidified to pH 2 with 5 M hydrochloric acid. The mixture was diluted with ethyl acetate and the aqueous layer was extracted with ethyl acetate (3×). The combined organic phase was dried with magnesium sulfate, filtered, and concentrated to afford the title compound as a solid (8.09 g, 89%); <sup>1</sup>H NMR (300 MHz, CDCl<sub>3</sub>) δ 1.36 (s, 9H), 7.54 (d,  $J = 8.4$  Hz, 2H), 7.61 (d,  $J = 5.1$  Hz, 1H), 7.92 (d,  $J = 8.4$  Hz, 2H), 8.34 (d,  $J = 5.1$  Hz, 1H), 11.04 (s, 1H); MS(FD)  $m/e$  303. Anal. (C<sub>16</sub>H<sub>17</sub>NO<sub>8</sub>S) C, H, N.

**2-(4-*tert*-Butylphenyl)-4H-thieno[3,2-*d*][1,3]oxazin-4-one (66).** To a mixture of compound **65** (8.09 g, 27 mmol) and methylene chloride (135 mL) was added oxalyl chloride (11.8 mL, 135 mmol). The mixture was heated until bubbling began, then stirred for 2 h without heating and concentrated. The residue was dissolved in methylene chloride (135 mL) and to this solution was added pyridine (2.2 mL, 27 mmol). After 1 h, the reaction mixture was concentrated and partitioned between ethyl acetate and water. The organic layer was washed with water (4×) and brine, the dried with MgSO<sub>4</sub> and concentrated. The residue was chromatographed over silica gel, eluting with 10% ethyl acetate/hexanes to afford the title compound as a solid (7.44 g, 96%); <sup>1</sup>H NMR (300 MHz, CDCl<sub>3</sub>) δ 1.37 (s, 9H), 7.35 (d,  $J = 5.1$  Hz, 1H), 7.52 (d,  $J = 8.4$  Hz, 2H), 7.91 (d,  $J = 5.1$  Hz, 1H), 8.22 (d,  $J = 8.4$  Hz, 2H); MS(FD)  $m/e$  285. Anal. (C<sub>16</sub>H<sub>15</sub>NO<sub>2</sub>S) C, H, N.

**3-(4-*tert*-Butylbenzoylamino)-N-(3-cyanophenyl)thiophene-2-carboxamide (67).** To a mixture of compound **66** (400 mg, 1.4 mmol), 3-aminobenzonitrile (165 mg, 1.4 mmol) and THF (5 mL) was added 0.5 M potassium hexamethyl disilazide in toluene (3.08 mL, 1.54 mmol) and stirred for 15 min. The reaction was diluted with aqueous NH<sub>4</sub>Cl and ethyl acetate. The organic layer was washed with water (3×) and brine, dried with MgSO<sub>4</sub> and concentrated. The residue was chromatographed over silica gel, eluting with 20% THF/hexanes, to give the title compound as a solid (580 mg, 51%); <sup>1</sup>N NMR (300 MHz, CD<sub>3</sub>OD) δ 1.37 (s, 9H), 7.47 (m, 4H), 7.57 (d,  $J = 8.4$  Hz, 2H), 7.68 (m, 1H), 7.98 (d,  $J = 8.4$  Hz, 2H), 8.20 (s, 1H), 8.42 (d,  $J = 5.7$  Hz, 1H), 11.80 (s, 1H); MS(FD)  $m/e$  403. Anal. (C<sub>23</sub>H<sub>21</sub>N<sub>3</sub>O<sub>2</sub>S) H, N; C: 67.83, calcd 68.46.

**3-(4-*tert*-Butylbenzoylamino)-N-[3-(aminoiminomethyl)phenyl]thiophene-2-carboxamide Hydrochloride (68).** Into a mixture of compound **67** (400 mg, 0.993 mmol), pyridine (10 mL), and triethylamine (1 mL) was bubbled hydrogen sulfide gas for 10 min. The solution was capped and allowed to stand overnight. The solvent was concentrated and the residue was dissolved in ethyl acetate and washed with water (2×) and saturated sodium bicarbonate. The organic layer was dried with MgSO<sub>4</sub>, filtered, and concentrated. The residue was dissolved in a mixture of 1:1 iodomethane:methanol (10 mL) and heated to reflux. After 30 min, the reaction was concentrated and the residue was vacuum-dried for 1 h. This residue was dissolved in a minimum amount of dry methanol and treated with ammonium acetate (230 mg, 2.98 mmol). The solution was heated to 65 °C for 1 h, cooled to room temperature, and the solution was triturated with diethyl ether and the solid was filtered off. The solid was dissolved in 10 mL of 1:1 tetrahydrofuran/water and treated with di-*tert*-butyl dicarbonate (1.08 g, 4.96 mmol) and potassium carbonate (822 mg, 5.96 mmol). After being stirred vigorously for 30 min, the solution was partitioned between ethyl acetate and water. The aqueous layer was extracted with ethyl acetate (2×) and the combined organic phase was dried with MgSO<sub>4</sub> and concentrated. The residue was chromatographed over silica gel, eluting with 30% ethyl acetate/dichloromethane to give 3-(4-*tert*-butylbenzoylamino)-N-[3-(*N*-*tert*-butoxycarbonylamino)(*N*-

*tert*-butoxycarbonylimino)methyl]phenyl]thiophene-2-carboxamide. This material was dissolved in trifluoroacetic acid (2 mL) and stirred for 1 h. The reaction was concentrated and the residue was dissolved in ethyl acetate. To this solution was added 1 M hydrochloric acid in ether, and the mixture was sonicated for 5 min. The resulting solid was filtered, dissolved in water, and lyophilized to afford the title compound as a powder (170 mg, 37%):  $^1\text{H NMR}$  (300 MHz, DMSO- $d_6$ )  $\delta$  1.38 (s, 9H), 7.56 (m, 1H), 7.63 (m, 3H), 7.83 (d,  $J = 8.29$  Hz, 2H), 7.96 (d,  $J = 5.27$  Hz, 1H), 8.05 (m, 1H), 8.16 (m, 2H); MS(FD)  $m/e$  421. Anal. ( $\text{C}_{23}\text{H}_{24}\text{N}_4\text{O}_2\text{S}\cdot 1.0\text{HCl}\cdot 0.8\text{H}_2\text{O}$ ) C, H, N.

**1-(Benzyloxycarbonylamino(benzyloxycarbonylimino)-methyl)piperidine-3-carboxylic Acid (70).** To a solution of nipecotic acid (1.66 g, 12.8 mmol) in 2 N NaOH (12.8 mL, 25.6 mmol) and dioxane (30 mL) was added compound **69** (4.6 g, 12.8 mmol). After 48 h, the reaction mixture was added to water (200 mL) and diethyl ether (200 mL). The aqueous layer was separated and extracted with diethyl ether ( $2 \times 200$  mL). The aqueous layer was acidified to pH 2.0 with 3 N HCl and extracted with ethyl acetate (500 mL). The organic layer was dried with  $\text{MgSO}_4$  and concentrated to give the title compound (4.0 g, 71%):  $^1\text{H NMR}$  (300 MHz,  $\text{CDCl}_3$ )  $\delta$  1.55–1.92 (m, 6H), 2.00–2.15 (m, 1H), 2.70–2.80 (m, 1H), 3.20–3.35 (q, 1H), 3.38–3.45 (m, 1H), 3.75–4.10 (m, 1H), 5.10 (s, 2H), 5.22 (s, 2H), 7.30–7.40 (m, 10H); MS(FD)  $m/e$  440 ( $\text{MH}^+$ ). Anal. ( $\text{C}_{23}\text{H}_{25}\text{N}_3\text{O}_6$ ) C, H, N.

**$N^1$ -[[1-(Aminoiminomethyl)piperidin-3-yl]carbonyl]- $N^2$ -(4-*tert*-butylbenzoyl)-1,2-benzenediamine Trifluoroacetate (71).** To a stirring solution of compound **70** (1.2 g, 2.7 mmol) in dichloromethane (30 mL) were added compound **14** (0.730 g, 2.7 mmol), 1,3-dicyclohexylcarbodiimide (0.556 g, 2.7 mmol), and 1-hydroxy-7-azabenzotriazole (0.367 g, 2.7 mmol). After stirring for 24 h, the precipitate was filtered and the filtrate was concentrated. The residue was dissolved in ethyl acetate (250 mL) and washed with 1 N  $\text{NaHCO}_3$ , water, and 1.5 N citric acid. The organic layer was dried with  $\text{MgSO}_4$  and concentrated. The residue was dissolved in ethanol (60 mL) and water (25 mL) was added, followed by 1 N HCl (5.0 mL, 5.0 mmol) and 5% Pd/C (1.5 g) and the stirring mixture was placed under an atmosphere of hydrogen (1 atm). After several hours, the catalyst was filtered through diatomaceous earth and the filtrate was concentrated and vacuum-dried overnight. The residue was dissolved in 0.1% TFA, filtered through a Millipore 0.5 mm filter, and chromatographed by RPHPLC on a  $5 \times 25$  cm column Vydac  $\text{C}_{18}$  resin (5% acetonitrile/water to 50% acetonitrile/water) to give the title compound as a white solid (0.550 g, 37%):  $^1\text{H NMR}$  (300 MHz, DMSO- $d_6$ )  $\delta$  1.33 (s, 9H), 1.3–2.0 (m, 4H), 2.6 (m, 1H), 3.09 (t,  $J = 11$  Hz, 1H), 3.25 (dd,  $J = 11, 13.5$  Hz, 1H), 3.75 (d,  $J = 13.5$  Hz, 1H), 3.80 (d,  $J = 13.5$  Hz, 1H), 7.15–7.25 (m, 2H), 7.35 (br s, 4H), 7.50–7.65 (m, 4H), 7.89 (d,  $J = 8.5$  Hz, 2H), 9.67 (s, 1H), 9.76 (s, 1H); MS(FAB)  $m/e$  422 ( $\text{MH}^+$ ). Anal. ( $\text{C}_{24}\text{H}_{34}\text{N}_5\text{O}_2\cdot 1.0\text{TFA}\cdot 1.0\text{H}_2\text{O}$ ) C, H, N.

**$N^1$ -[[1-(Aminoiminomethyl)piperidin-3-yl]carbonyl]- $N^2$ -(4-methoxybenzoyl)-1,2-benzenediamine Trifluoroacetate (72).** Following the procedure described for the synthesis of compound **71**, **72** was prepared from compound **13** and compound **70**: 75% yield;  $^1\text{H NMR}$  (300 MHz, DMSO- $d_6$ )  $\delta$  1.40 (m, 1H), 1.60 (m, 2H), 2.00 (m, 1H), 2.65 (m, 1H), 3.08 (t,  $J = 11.1$  Hz, 1H), 3.24 (dd,  $J = 10.6, 13.6$  Hz, 1H), 3.74 (d,  $J = 13.6$  Hz, 1H), 3.84 (s, 3H), 3.90 (d,  $J = 13.6$  Hz, 1H), 7.08 (d,  $J = 9.0$  Hz, 2H), 7.20–7.30 (m, 2H), 7.37 (br s, 4H), 7.50–7.55 (m, 1H), 7.60–7.65 (m, 1H), 7.94 (d,  $J = 9.0$  Hz, 2H), 9.69 (s, 1H), 9.71 (s, 1H); MS(FAB)  $m/e$  396.2 ( $\text{MH}^+$ ). Anal. ( $\text{C}_{21}\text{H}_{25}\text{N}_5\text{O}_3\cdot 1.1\text{TFA}\cdot 0.5\text{H}_2\text{O}$ ) C, H, N.

**Molecular Modeling.** The protein structure coordinate set used in this investigation was the human fXa X-ray structure reported by Padmanabhan et al.<sup>13</sup> (Brookhaven PDB file 1hcg). The supplied chymotrypsinogen residue numbering<sup>18</sup> was maintained. The computational construction of ligands and protein–ligand complexes and the graphical analysis of results were performed with QUANTA, version 96.<sup>27</sup> Energy minimization was performed using CHARMM, version 23.2.<sup>27,28</sup> Details of the initial computational preparation of the fXa

X-ray protein structure used in this study are described in ref 10. Briefly this initial protein system consists of all residues (explicit hydrogens), an 8 Å surface solvation shell, a more extensive active site solvation (a 20 Å sphere centrally located), and minimal processing by constrained energy minimization to refine hydrogen positions and to relieve severe close contacts. This initial protein system coordinate set was used as the starting structure for the rigid body docking of **1** and the construction of all subsequent protein–ligand complexes modeled. Energy evaluation and minimization were done using the same nonbond settings and algorithm criteria as reported in ref 10.

The computational exploration of the fXa active site for potential binding modes of **1** was performed using a significantly modified version of the program SUPER.<sup>29</sup> SUPER was originally designed to systematically search for the best superposition of two rigid molecules, based upon a calculated dot correspondence of their respective surfaces. This dot correspondence is an indirect measure of the similarity in shape of two molecules that can further be qualified by the electrostatic potential. In a total reengineering of the program we incorporated the ability to perform the inverse matching operation, namely to search for the best superposition that maximizes the correspondence of the “complement” of two molecular surfaces. This is primarily achieved by incorporating a severe penalty for atom close contacts. This is in effect now a docking method since either (or both) of the two molecules can be a protein. Among other relevant program changes added are the abilities to define a subset of the molecular surface to consider, to systematically position one molecule (ligand) on the surface of the second (protein), and to utilize multiple conformations of the ligand. The united atom restriction has been removed and an alternative Monte Carlo method to generate different orientations of the ligand has been incorporated. As in the original SUPER program, a collection of solutions are obtained and rank ordered according to their dot correspondence score.

In the current docking study we were only interested in obtaining a collection of general binding modes for this unique molecular scaffold (**1**), to be used as suggestions for analogue design. Therefore at this stage we chose to only use the steric criteria to score the results.<sup>29</sup> The 3D ligand structure of **1** was built in the ChemNote drawing facility using default atom types and smoothing assigned charges over all C and nonpolar H atoms to give a total sum of 0.0. To expedite the docking process, only a small number of ligand conformations were used. From an extensive systematic conformational search of all rotatable bonds (non-terminal and non-amide), it was decided that four “ideal” conformations of **1** would be used to represent the conformational space available to the bisamide phenyl scaffold. Considering the two amide bonds, these conformations can be described as pseudo-antiparallel, pseudo-parallel, C7-ring hydrogen-bonded, and C7-ring un-hydrogen-bonded. For each, the lowest energy combination for the positions of two methoxy groups (either 0° or 180°) was used. The region of the fXa protein surface explored included all exposed residues having at least one atom within 14 Å of a point central to the active site. For the docking operation all waters were removed from the protein, and no side chain conformational changes were considered. The running parameters used in the docking calculations included a 0.5 Å surface dot spacing, a protein surface sampling interval of every four dots (2 Å), and 25 Monte Carlo orientations of **1** generated for each conformation, at each protein surface point sampled. A total of 492400 fXa binding modes of **1** were evaluated (123100/conformation). The top 20 scoring modes were visually examined; from the top five, three distinct forms were found to exist. These general binding modes are illustrated in Figure 2 as model I, model II, and model III.

Visual inspection of model I revealed that a symmetrically related, but under represented, conformation of **1** would introduce the possibility for forming at least one hydrogen bond with the protein. This conformational change was accomplished by manually rotating 180° about the CN bond emanat-

ing from the central ring (C-ring), for both the A- and B-chains, while leaving the central ring unmodified. This intermediate, unrefined binding mode for **1** served as the template to build all other analogues modeled (**2**, **3**, and **44**). Each ligand was constructed by modifying **1** using the 3D Editor, smoothing assigned charges to give a total sum of +1.0. All were then processed by reinserting each analogue into the active site of the fully solvated fXa protein starting structure and deleting waters having a oxygen within 2.0 Å of a ligand atom. The active site complex of each was then energy minimized using the same constraint regime reported in ref 10. The final energy-minimized structure for **2** (green) and **3** (purple) is shown in Figure 3, and the processed complex for **44** appears in Figure 4. In both Figures 3 and 4, all aliphatic hydrogens and waters have been removed for clarity.

**X-ray Crystallography.** The human  $\alpha$ -thrombin was co-crystallized with the inhibitor in the active site and hirugen bound in the exo-site using conditions previously described.<sup>21</sup> Obtained crystals belong to the C2 space group with unit cell constants  $a = 71.4$  Å,  $b = 71.9$  Å,  $c = 73.7$  Å,  $\beta = 101.0^\circ$  and have one molecular complex per asymmetric unit. An X-ray data set was collected using a conventional rotating anode with Cu K $\alpha$  radiation ( $\lambda = 1.54$  Å). An imaging plate (R-AXISII) was used as a detector. A total of 87777 observations were measured and yielded 20636 unique reflections with an  $R_{\text{merge}}$  of 5.5% (18.7% for outer shell). This represents 96% of all reflections that are theoretically possible for the resolution range of 30–2.1 Å. A final crystallographic  $R$ -value of 18.9% was obtained for 20469 reflections, with  $F > 2\sigma$  in the 20–2.1 Å resolution range. An  $R_{\text{free}}$  of 22.4% was calculated, using a random selection of approximately 4% of the data not involved in the crystallographic refinement. The root-mean-square deviation from ideal bond lengths was 0.009 Å, that from ideal angles 1.4°. Model inspection and correction between cycles of the refinement and crystallographic refinement itself were performed within the QUANTA97 and X-PLOR98 program suites. The position of **44** in the active site was assigned based on the electron density distribution after four rounds of refinement. Well-defined electron density covered every portion of the inhibitor, clearly indicating a single binding mode.

**Enzyme Affinity and Anticoagulant Activity.** The binding affinities for human fXa (and other serine proteases) were measured as apparent association constants ( $K_{\text{ass}}$ ) derived from protease inhibition kinetics as described previously.<sup>22b,30,31</sup> The apparent  $K_{\text{ass}}$  values were obtained in a high-volume testing protocol using automated dilutions of inhibitors (performed in triplicate at each of four to eight inhibitor concentrations) into 96-well plates and chromogenic substrate hydrolysis rates determined at 405 nm using a Thermomax plate reader from Molecular Devices (San Francisco, CA). In the fXa assay protocol, 25  $\mu\text{L}$  inhibitor test solution (in MeOH) was added to 50  $\mu\text{L}$  buffer (0.06 M tris, 0.3 M NaCl, pH 7.4), followed by the addition of 25  $\mu\text{L}$  human fXa (32 nM in 0.03 M tris, 0.15 M NaCl, 1 mg/mL HSA). Finally, 150  $\mu\text{L}$  substrate solution (0.3 mM in water) was added within 2 min to start hydrolysis. The final fXa concentration was 3.2 nM. The concentrations of free fXa and bound fXa were determined from linear standard curves on the same plate by use of SoftmaxPro software for each inhibitor concentration and the apparent  $K_{\text{ass}}$  was calculated for each inhibitor concentration which produced hydrolysis inhibition between 20% and 80% of the control (3.2 nM fXa): apparent  $K_{\text{ass}} = [\text{E}]/[\text{E}_0][\text{I}] = [\text{E}_b]/[\text{E}_f][\text{I}^0 - \text{I}_b]$ . This method allows affinity determinations for tight binding enzyme inhibitors as well as for weak binding inhibitors and has generated a large protease inhibitor SAR database.<sup>11a,22,30–32</sup>

This system of affinity measurement was designed to (1) validly assess a very large number of protease inhibitor samples and (2) determine affinity with tight binding inhibitors where classical  $K_i$  methods fail.<sup>33</sup> Algebraic solutions for the equation  $K_{\text{ass}} = [\text{E}]/[\text{E}_0][\text{I}] = [\text{E}_b]/[\text{E}_f][\text{I}^0 - \text{I}_b]$  account for the free and bound inhibitor concentrations. Alternatively, the whole data set can be graphically analyzed as a linearized solution to the same  $K_{\text{ass}}$  equation:  $\text{I}^0(1 - a) = [1/(\text{apparent } K_{\text{ass}})(a) + \text{E}^0]$ , where  $a = \text{fraction of free enzyme}$ .<sup>31a</sup> This

equation was also derived by Henderson<sup>33a</sup> and Beith<sup>33b</sup> for study of tight binding inhibitors, where classical methods fail to account for bound inhibitor concentrations. The application of this method has facilitated the accumulation of a large database of apparent  $K_{\text{ass}}$  values (obtained at a single appropriate substrate concentration with each protease of interest) which are self-consistent for each protease. These data can be used to assess selectivity by directly comparing the  $K_{\text{ass}}$  values for respective proteases. Apparent  $K_{\text{ass}}$  values can be corrected by determining the effect of substrate concentration<sup>31a,33</sup> (apparent  $K_{\text{ass}} = 1/\text{apparent } K_i$ ; corrected  $K_{\text{ass}} = 1/K_i$ ). The variability of mean apparent  $K_{\text{ass}}$  values determined at the single substrate concentration was  $\pm 15\%$ . The assay system  $K_m$  was measured as  $0.347 \pm 0.031$  mM ( $n = 4$ ), and  $V_{\text{max}}$  was  $13.11 \pm 0.76$   $\mu\text{M}/\text{min}$ . For classical  $K_i$  determinations Dixon plots were generated with the same protocol using four substrate concentrations (0.112, 0.224, 0.448, 0.896 mM), and the type of inhibition was confirmed with Lineweaver–Burke graphs.

Anticoagulant activity, measured as prothrombin times (PT) or activated partial thromboplastin times (APTT), were evaluated as previously described.<sup>22b,30</sup>

**Prothrombin Time Assay for Species Comparison and Animal Studies.** PT was determined with a fibrometer for comparison of PT responses in plasma from rabbit, rat, and dog. Reconstituted human plasma (citrol; Dade, Miami, FL) was used. One part (100  $\mu\text{L}$ ) plasma, one part normal saline, and one part PT reagent (rabbit brain thromboplastin, Dade Thromboplastin C Plus) were added to the fibrometer cup and the timer was triggered. Each concentration for each species was assayed in duplicate; the average was divided by the respective control PT and expressed as PT ratio. Plasma was collected in 3.8% sodium citrate (1 part citrate to 9 parts blood) from at least three animals of each species and was pooled, frozen and thawed for use. Each compound was assayed three separate times in pooled plasma from each species. Results were expressed as means  $\pm$  SEM for each dose group.

**Model of Extracorporeal Arteriovenous Shunt Thrombosis in the Rat and Rabbit.** The extracorporeal arteriovenous (AV) shunt thrombosis model described by Smith and White<sup>26a</sup> and Ashida et al.<sup>26b</sup> was used in rats to evaluate the antithrombotic efficacy of anticoagulants in a model of extracorporeal circulation. Male Sprague–Dawley rats weighing 325–400 g (Harlan Sprague–Dawley Inc., Indianapolis, IN) were anesthetized with a combination of xylazine (30 mg/kg, sc) and ketamine (150 mg/kg, sc) and were laid on a heating pad (37 °C). Briefly, the AV shunt consisted of three pieces of polyethylene (PE) tubing. Segments of tubing (PE 60, 20 cm long) were implanted in the right carotid artery and the left jugular vein. A center segment (PE 190, 6 cm long) was friction fitted between the arterial and venous sections. The center segment contained a length of mercerized cotton thread (6.5 cm) with one end that was friction fitted at the junction of the arterial to center segments and the opposite end was free floating. The length of thread that was in contact with fluid in the tubing was 5 cm long. The shunt tubing was filled with normal saline. The carotid artery was clamped with a microvascular clamp except while blood was allowed to flow through the shunt. Blood flowed through the shunt for 15 min. Then, the carotid was clamped and the center section of tubing was removed from the circuit. The short section was held vertically, the thread was removed carefully to avoid loss of thrombotic material on the side of the tubing, and the thread was weighed on an analytical balance. Ten 6.5 cm lengths of thread were soaked in saline and weighed. The average weight of the wet thread (5.5 mg) was subtracted from the total weight of a thread removed from the shunt of an experimental animal. Vehicle or drug solution was infused continuously through a catheter implanted in a right jugular vein and advanced 1 cm into the vein. A second catheter, for blood sampling, was also implanted in the right jugular vein but was advanced 6 cm to position the tip below the junction of the vena cava and the right atrium to prevent contamination of samples with un-equilibrated blood flowing past the infusion catheter. The

positions of the tips of the infusion and sampling catheters were documented after experiments in initial studies.

The experimental protocol for the rabbit was the same except for the following differences. Male New Zealand white rabbits weighing 2.5–3 kg (Myrtle Rabbitry, Inc., Thompson Station, TN) were anesthetized with a combination of xylazine (25 mg/kg, sc) and ketamine (100 mg/kg, sc) and were laid on a heating pad (37 °C). The tubing (PE 200) implanted into the carotid and the jugular was 26 cm long and the center section (PE 260) was 6.5 cm long. The thread in the shunt consisted of four strands each 7.5 cm long with a single knot tied at the end of the group. The length of the thread exposed to fluid was 6 cm and the knot was positioned 2 mm from the venous end of the center section. The average wet weight of the thread was 38 mg ( $n = 10$ ) which was subtracted from the total weight of the thread and thrombotic material. The tip of the infusion catheter was implanted 2 cm and the tip of the sampling catheter was advanced 15 cm to a position below the heart.

Drugs were prepared fresh daily in isotonic saline (D-1-Piq-Pro-ArgH) or 15% DMSO in normal saline. Vehicle or drug solutions were infused continuously iv with a syringe pump starting 15 min before and continuing throughout the 15-min period of blood circulation through the shunt. The infusion volume was 6 mL/h in rats and 25 mL/h in rabbits. A minimum of four animals for each dose group were studied.

**Acknowledgment.** The authors thank Dr. Matthew J. Fisher for many helpful discussions. V.J.K. would like to thank Dr. Robert B. Hermann for providing the SUPER program and helpful discussions. The reengineering of SUPER is gratefully acknowledged by V.J.K. as a collaboration with Michael A. Heathman, who provided all the software development effort and many ideas for algorithm enhancement.

**Supporting Information Available:** Abbreviated procedures for the synthesis of intermediates **10**, **11**, **14**, **15**, **18–24**, **26–28**, **31**, **33**, **35–43**, **55**, **56**, **58–61**, and **64**. These compounds were prepared by methods substantially equivalent to those described for the representative examples presented herein. This material is available free of charge via the Internet at <http://pubs.acs.org>.

## References

- (1) (a) Vacca, J. P. Thrombosis and coagulation. *Annu. Rep. Med. Chem.* **1998**, *33*, 81–90. (b) Ripka, W. C.; Vlasuk, G. P. Antithrombotics – serine proteases. *Annu. Rep. Med. Chem.* **1997**, *32*, 71–89.
- (2) (a) Meade, W. M.; Miller, G. J.; Rosenberg. Characteristics Associated with the Risk of Arterial Thrombosis. In *Cardiovascular Thrombosis: Thrombocardiology and Thrombology*, 2nd ed.; Verstraete, M., Fuster, V., Topol, E. J., Eds.; Lippincott-Raven Publishers: Philadelphia, 1998; pp 77–89. (b) Carter, C. J.; Samama, M. M. Characteristics Associated with the Risk of Venous Thrombosis. In *Cardiovascular Thrombosis: Thrombocardiology and Thrombology*, 2nd ed.; Verstraete, M., Fuster, V., Topol, E. J., Eds.; Lippincott-Raven Publishers: Philadelphia, 1998; pp 91–102.
- (3) (a) Amerena, J.; Mashford, M. L.; Wallace, S. Adverse effects of anticoagulants. *Adverse Drug React. Acute Poisoning Rev.* **1990**, *9*, 1–36. (b) Levine, M. N.; Hirsh, J.; Salzman, E. W. Side effects of antithrombotic therapy. In *Hemostasis and Thrombosis: Basic Principles and Clinical Practice*, Colman, R. W., Hirsh, J., Marder, V. J., Salzman, E. W., Eds.; J. B. Lippincott Co.: Philadelphia, 1994; pp 936–955. (c) Williams, E. C.; Suttie, J. W. Vitamin K antagonists. In *Cardiovascular Thrombosis: Thrombocardiology and Thrombology*; Verstraete, M., Fuster, V., Topol, E. J., Eds.; Lippincott-Raven: Philadelphia, 1998; pp 285–300. (d) Hirsh, J. Oral Anticoagulants. *N. Engl. J. Med.* **1991**, *324*, 1865–1875.
- (4) Wiley, M. R.; Fisher, M. J. Small-molecule direct thrombin inhibitors. *Exp. Opin. Ther. Patents* **1997**, *7* (11), 1265–1282.
- (5) Lawson, J. H.; Kalafatis, M.; Stram, S.; Mann, K. G. A model for the tissue factor pathway to thrombin. *J. Biol. Chem.* **1994**, *269* (37), 23357–23366.
- (6) Vlasuk, G. P. Structural and Functional Characterization of Tick Anticoagulant Peptide (TAP): A Potent and Selective Inhibitor of Blood Coagulation Factor Xa. *Thromb. Haemostasis* **1993**, *70* (1), 212–216.
- (7) Schaffer, L. W.; Davidson, J. T.; Vlasuk, G. P.; Dunwiddie, C. T.; Siegl, P. K. S. Selective Factor Xa Inhibition by Recombinant Antistasin Prevents Vascular Graft Thrombosis in Baboons. *Arterioscl. Thromb.* **1992**, *12*, 879–885.
- (8) Wong, A. G.; Gunn, A. C.; Ku, P.; Hollenbach, S. J.; Sinha, U. Relative Efficacy of Active Site-Blocked Factors IXa, Xa in Models of Rabbit Venous and Arterio-Venous Thrombosis. *Thromb. Haemostasis* **1997**, *77*, 1143–1147.
- (9) G. F. Smith, Lilly Research Laboratories, unpublished results.
- (10) Herron, D. K.; Goodson, T., Jr.; Wiley, M. R.; Weir, L. C.; Kyle, J. A.; Yee, Y. K.; Tebbe, A. L.; Tinsley, J. M.; Mendel, D.; Masters, J. J.; Franciskovich, J. B.; Sawyer, J. S.; Beight, D. W.; Ratz, A. M.; Milot, G.; Hall, S. E.; Klimkowski, V. J.; Wikel, J. H.; Eastwood, B. J.; Towner, R. D.; Gifford-Moore, D.; Craft, T. J.; Smith, G. F. 1,2-Dibenzamido benzene Inhibitors of Human Factor Xa. *J. Med. Chem.* **2000**, *43*, 859–872.
- (11) (a) Wiley, M. R.; Chirgadze, N. Y.; Clawson, D. K.; Craft, T. J.; Gifford-Moore, D. S.; Jones, N. D.; Olkowski, J. L.; Weir, L. C.; Smith, G. F. D-Phe-Pro-p-amidinobenzylamine: a potent and highly selective thrombin inhibitor. *Bioorg. Med. Chem. Lett.* **1996**, *6* (20), 2387–2392. (b) Sturzebecher, J.; Markwardt, F.; Viogt, B.; Wagner, G.; Walsmann, P. Cyclic amides of N- $\alpha$ -arylsulfonylamino-acylated-4-amidinophenylalanine: tight binding inhibitors of thrombin. *Thromb. Res.* **1983**, *29*, 635–642.
- (12) (a) Nagahara, T.; Yokoyama, Y.; Inamura, K.; Katakura, S.; Komoriya, S.; Yamaguchi, H.; Hara, T.; Iwamoto M. Dibasic (amidinoaryl)propanoic acid derivatives as novel blood coagulation factor Xa inhibitors. *J. Med. Chem.* **1994**, *37*, 1200–1207. (b) Quan, M. L.; Pruitt, J. R.; Ellis, C. D.; Liaw, A. Y.; Galemno, R. A. Jr.; Stouten, P. F. W.; Wityak, J.; Knabb, R. M.; Thoolen, M. J.; Wong, P. C.; Wexler, R. R. Bisbenzamide isoxazoline derivatives as factor Xa inhibitors. *Bioorg. Med. Chem. Lett.* **1997**, *7*, 2813–2818. (c) Shaw, K. J.; Guilford, W. J.; Dallas, J. L.; Koovakkaat, S. K.; McCarrick, M. A.; Liang, A.; Light, D. R.; Morrissey, M. M. (Z,Z)-2,7-Bis(4-amidinobenzylidene) cycloheptan-1-one: Identification of a Highly Active Inhibitor of Blood Coagulation Factor Xa. *J. Med. Chem.* **1998**, *41*, 3551. (d) Philips, G. B.; Buckman, B. O.; Davey, D. D.; Eagen, K. A.; Guilford, W. J.; Hinchman, J.; Ho, E.; Koovakkaat, S.; Liang, A.; Light, D. R.; Mohan, R.; Ng, H. P.; Post, J. M.; Shaw, K. J.; Smith, D.; Subramanyam, B.; Sullivan, M. E.; Trinh, L.; Vergona, R.; Walters, J.; White, K.; Whitlow, M.; Wu, S.; Xu, W.; Morrissey, M. M. Discovery of N-[2-[5-[Amino(imino)methyl]-2-hydroxyphenoxy]-3,5-difluoro-6-[3-(4,5-dihydro-1-methyl-1H-imidazol-2-yl)phenoxy]pyridin-4-yl]-N-methylglycine (ZK-807834): A Potent, Selective and Orally Active Inhibitor of the Blood Coagulation Enzyme Factor Xa. *J. Med. Chem.* **1998**, *41*, 3557. (e) Gabriel, B.; Stubbs, M. T.; Bergner, A.; Hauptmann, J.; Bode, W.; Sturzebecher, J.; Maroder, L. Design of benzamide-type inhibitors of factor Xa. *J. Med. Chem.* **1998**, *41*, 4240–4250. (f) Kuczniarz, R.; Grams, F.; Leinert, H.; Marzenell, K.; Engh, R. A.; von der Saal, W. Tetrahydroisoquinoline-based factor Xa inhibitors. *J. Med. Chem.* **1998**, *41*, 4983–4994. (g) Galemno, R. A., Jr.; Maduskie, T. P.; Dominguez, C.; Rossi, K. A.; Knabb, R. M.; Wexler, R. R.; Stouten, P. F. W. The de novo design and synthesis of cyclic urea inhibitors of factor Xa: initial SAR studies. *Bioorg. Med. Chem. Lett.* **1998**, *8*, 2705–2710. (h) Buckman, B. O.; Mohan, R.; Koovakkaat, S.; Liang, A.; Trinh, L.; Morrissey, M. M. Design, synthesis and biological activity of novel purine and bicyclic pyrimidine factor Xa inhibitors. *Bioorg. Med. Chem. Lett.* **1998**, *8*, 2235.
- (13) Padmanabhan, K.; Padmanabhan, K. P.; Tulinsky, A.; Park C. H.; Bode, W.; Huber, R.; Blankenship, D. T.; Cardin, A. D.; Kisel W. Structure of human des(1–45) Factor Xa at 2.2 Å resolution. *J. Mol. Biol.* **1993**, *232*, 947–966.
- (14) Yee, Y. K.; Tebbe, A. L.; Linebarger, J. H.; Beight, D. W.; Craft, T. J.; Gifford-Moore, D. S.; Goodson, T., Jr.; Herron, D. K.; Klimkowski, V. J.; Kyle, J. A.; Sawyer, J. S.; Smith, G. F.; Tinsley, J. M.; Towner, R. D.; Weir, L. C.; Wiley, M. R. N<sup>2</sup>-Aroylanthranilamide Inhibitors of Human Factor Xa. *J. Med. Chem.* **2000**, *43*, 873–882.
- (15) Fisher, M. J.; Gunn, B.; Harms C. S.; Kline, A. D.; Mullaney, J. T.; Nunes A.; Scarborough, R. M.; Arfsten, A. E.; Skelton, M. A.; Um S. L.; Utterback, B. G.; Jakubowski, J. A. Non-peptide RDG surrogates which mimic a Gly-Asp  $\beta$ -turn: potent antagonists of platelet glycoprotein IIb/IIIa. *J. Med. Chem.* **1997**, *40*, 2085–2101.
- (16) Judkins, B. D.; Allan, D. G.; Cook, T. A.; Evans, B.; Sardharvala, T. E. *Synth. Commun.* **1996**, *26* (23), 4351–4367.
- (17) (a) Baker, E. N.; Hubbard, R. E. Hydrogen bonding in globular proteins. *Prog. Biophys. Mol. Biol.* **1984**, *44*, 97–197. (b) McDonald, I. K.; Thornton, J. M. Satisfying hydrogen bonding potential in proteins. *J. Mol. Biol.* **1994**, *238*, 777–793.
- (18) Bode, W.; Turk, D.; Karshikov, A. The refined 1.9 X-ray crystal structure of D-Phe-Pro-Arg chloromethyl ketone-inhibited human  $\alpha$ -thrombin. Structure analysis, overall structure, electrostatic properties, detailed active-site geometry, structure–function relationships. *Protein Sci.* **1992**, *1*, 426–471.

- (19) (a) Chow, M. M.; Meyer, E. F., Jr.; Bode, W.; Kam, C.-M.; Radhakrishnan, R.; Vijayalakshmi, J.; Powers, J. C. The 2.2Å resolution X-ray crystal structure of the complex of trypsin inhibited by 4-chloro-3-ethoxy-7-guanidinocoumarin: A proposed model of the thrombin-inhibitor complex. *J. Am. Chem. Soc.* **1990**, *112*, 7783–7789. (b) Bode, W.; Truk, D.; Sturzebecher, J. Geometry of binding of the benzamidine- and arginine-based inhibitors NAPAP and MQPA to human  $\alpha$ -thrombin. X-ray crystallographic determination of the NAPAP-trypsin complex and modeling of NAPAP-thrombin and MQPA-thrombin. *Eur. J. Biochem.* **1990**, *193*, 175–182.
- (20) Renatus, M.; Bode, W.; Huber, R.; Sturzebecher, J.; Stubbs, M. T. Structural and functional analyses of benzamidine-based inhibitors in complex with trypsin: implications for the inhibition of factor Xa, tPA, and urokinase. *J. Med. Chem.* **1998**, *41*, 5445–5456.
- (21) Chirgadze, N. Y.; Sall, D. J.; Hermann, R.; Clawson, D. K.; Klimkowski, V. J.; Smith, G. F.; Gifford-Moore, D. S.; Coffman, W. J. The crystal structure of human  $\alpha$ -thrombin complexed with LY178550, a nonpeptidyl, active-site directed inhibitor. *Protein Sci.* **1997**, *6* (7), 1412–1417.
- (22) (a) Wiley, M. R.; Chirgadze, N. Y.; Clawson, D. K.; Craft, T. J.; Gifford-Moore, D. S.; Jones, N. D.; Olkowski, J. L.; Schacht, A. L.; Weir, L. C.; Smith, G. F. The serine protease selectivity of the thrombin inhibitor D-Phe-Pro-Arginine and its homologues. *Bioorg. Med. Chem. Lett.* **1995**, *5* (3), 2835–2840. (b) Smith, G. F.; Shuman, R. T.; Craft, T. J.; Gifford-Moore, D. S.; Kurz, K. D.; Jones, N. D.; Chirgadze, N.; Hermann, R. B.; Coffman, W. J.; Sandusky, G. E.; Roberts, E.; Jackson, C. V. A family of arginal thrombin inhibitors related to efegatran. *Sem. Thromb. Hemostasis* **1996**, *22* (2), 173–183.
- (23) Katakura, S.; Nagahara, T.; Hara, T.; Iwamoto, M. A novel factor Xa inhibitor: structure–activity and selectivity between factor Xa and thrombin. *Biochem. Biophys. Res. Commun.* **1995**, *30*, 387–394.
- (24) (a) Shuman, R. T.; Rothenberger, R. B.; Jackson, C. V.; Roberts, E. W.; Singer, B.; Lucas, R. A.; Kurz, K. D. Oral activity of tripeptide aldehyde thrombin inhibitors. In *Peptides: Chemistry, Structure and Biology*; Pravin, Kaumaya, T. P., Hodges, R. S., Eds.; Mayflower Scientific Ltd., 1996; p 215. (b) Shuman, R. T.; Rothenberger, R. B.; Campbell, C. S.; Smith, G. F.; Gifford-Moore, D. S.; Paschal, J. W.; Geselchen, P. D. Structure activity study of tripeptide thrombin inhibitor using  $\alpha$ -alkyl amino acids and other conformationally constrained amino acid substitutions. *J. Med. Chem.* **1995**, *38*, 4446–4453.
- (25) The species selectivity profile reported here is similar to that reported for DX-9065a. In the DX-9065a study, fXa from other species was isolated and evaluated to demonstrate that differences in enzyme affinity were responsible for the differences in anticoagulant activity. Hara, T.; Kunitada, S.; Iwamoto, M. DX-9065a, a synthetic and selective factor Xa inhibitor: species difference in its anticoagulant activity. *Thromb. Haemostasis* **1993**, *69*, 890 (Suppl.).
- (26) (a) Smith, J. R.; White, A. M. Fibrin, red cell and platelet interactions in an experimental model of thrombosis. *Br. J. Pharmacol.* **1982**, *77*, 29–38. (b) Ashida, S.; Sakuma, K.; Abido, Y. Antithrombotic effects of ticlopidine, acetylsalicylic acid and dipyridamole in vascular shunt model in rats. *Thromb. Res.* **1980**, *17*, 663–671.
- (27) Molecular Simulations Inc., 9685 Scranton Rd., San Diego, CA 92121.
- (28) Brooks, B. R.; Bruccoleri, R. E.; Olafson, B. D.; States, D. J.; Swaminathan, S.; Karplus, M. CHARMM: A Program for Macromolecular Energy, Minimization, and Dynamics Calculations. *J. Comput. Chem.* **1983**, *4*, 187–217.
- (29) Hermann, R. B.; Herron, D. K. OVID and SUPER: Two overlap programs for drug design. *J. Comput.-Aided Mol. Des.* **1991**, *5*, 511–524.
- (30) Sall, D. J.; Bastian, J. A.; Briggs, S. L.; Buben, J. A.; Clawson, D. K.; Denney, M. L.; Giera, D. D.; Gifford-Moore, D. S.; Harper, R. W.; Hauser, K. L.; Klimkowski, V. J.; Kohn, T. J.; Lin, H.-S.; McCowan, J. R.; Palkowitz, A. D.; Smith, G. F.; Takeuchi, K.; Thrasher, K. J.; Tinsley, J. M.; Utterback, B. G.; Yan, S.-C. B.; Zhang, M. Dibasic benzo[b]thiophene derivatives as a novel class of active site-directed thrombin inhibitors. 1. Determination of the serine protease selectivity, structure–activity relationships, and binding orientation. *J. Med. Chem.* **1997**, *40* (22), 3489–3493.
- (31) (a) Smith, G. F.; Gifford-Moore, D. S.; Craft, T. J.; Chirgadze, N.; Ruterbories, K. J.; Lindstrom, T. D.; Satterwhite, J. H. Efegatran: A New Cardiovascular Anticoagulant. In *New Anticoagulants for the Cardiovascular Patient*; Pifarre, R., Ed.; Hanley & Belfus, Inc.: Philadelphia, 1997; pp 265–300. (b) Sall, D. J.; Bastian, J. A.; Chirgadze, N. Y.; Denny, M. L.; Fisher, M. J.; Gifford-Moore, D. S.; Harper, R. W.; Klimkowski, V. J.; Kohn, T. J.; Lin, H. S.; McCowan, J. R.; Richett, M. E.; Smith, G. F.; Takeuchi, K.; Toth, J. E.; Zhang, M. Diaminobenzo[b]thiophene derivatives as a novel class of active site directed thrombin inhibitors: 5. Potency, efficacy and pharmacokinetic properties of modified C-3 side chain derivatives. *J. Med. Chem.* **2000**, *43*, 649–663.
- (32) (a) Sall, D. J.; Briggs, S. L.; Clawson, D. K.; Gifford-Moore, D. S.; Klimkowski, V. J.; McCowan, J. R.; Smith, G. F.; Wikel, J. H. Dibasic benzo[b]thiophenes derivatives as a novel class of active site directed thrombin inhibitors. 2. exploring interactions at the proximal (S2) binding site. *Bioorg. Med. Chem. Lett.* **1998**, *8*, 2527–2532. (b) Chirgadze, N. Y.; Sall, D. J.; Briggs, S. L.; Clawson, D. K.; Zhang, M.; Smith, G. F.; Schevitz, R. W. The crystal structures of human  $\alpha$ -thrombin complexed with active site-directed diamino benzo[b]thiophene derivatives: a novel binding mode for a structurally unique class of inhibitors. *Protein Sci.* **1999**, in press. (c) Schacht, A. L.; Chirgadze, N.; Clawson, D.; Craft, T. J.; Coffman, W. J.; Jones, N. D.; Gifford-Moore, D. S.; Olkowski, J.; Shuman, R. T.; Smith, G. F.; Weir, L. C.; Wiley, M. R. N-Substituted glycines as replacements for proline in tripeptide aldehyde thrombin inhibitors. *Bioorg. Med. Chem. Lett.* **1995**, *5*, 2529–2534. (d) Johnson, M. G.; Bronson, D. D.; Gillispie, J. E.; Gifford-Moore, D. S.; Kalter, K.; Lynch, M. P.; McGowan, J. R.; Redick, C. C.; Sall, D. J.; Smith, G. F.; Fogelsson, R. J. Solid-phase chemistry approach to the SAR development of a novel class of active site-directed thrombin inhibitors. *Tetrahedron* **1999**, *55*, 11641–11652. (e) Bastian, J. A.; Sall, D. J.; Chirgadze, N. Y.; Denny, M. L.; Gifford-Moore, D. S.; Smith, G. F.; Wikel, J. H. Diamino benzo[b]thiophenes derivatives as a novel class of active site directed thrombin inhibitors. 3. Enhancing activity by imposing conformational restriction in the C-4 side chain. *Bioorg. Med. Chem. Lett.* **1999**, *8*, 363–368. (f) Takeuchi, K.; Kohn, T. J.; Sall, D. J.; Denny, M. L.; McCowan, J. R.; Smith, G. F.; Gifford-Moore, D. S. Dibasic benzo[b]thiophene derivatives as a novel class of active site directed thrombin inhibitors: 4. SAR studies on the conformationally restricted C3-side chain of hydroxybenzo[b]thiophenes. *Bioorg. Med. Chem. Lett.* **1999**, *9*, 759–764. (g) Wiley, M. R.; Weir, L. C.; Briggs, S. L.; Chirgadze, N. Y.; Clawson, D.; Gifford-Moore, D. S.; Schacht, A. L.; Smith, G. F.; Vasudevan, V.; Zornes, L. L.; Klimkowski, V. J. The design of potent, selective, non-covalent, peptide thrombin inhibitors utilizing imidazole as a S1 binding element. *Bioorg. Chem. Med. Lett.* **1999**, *9*, 2767–2772.
- (33) (a) Henderson, P. J. F. A linear equation that describes the steady-state kinetics of enzymes and subcellular particles interacting with tightly bound inhibitors. *Biochem. J.* **1972**, *127*, 321–333. (b) Bieth, J. G. Pathophysiological interpretation of kinetic constants of protease inhibitors. *Bull. Eur. Physiopath. Resp.* **1980**, *16* (Suppl.), 183–195.